Evolutionary genomics predicts adaptive genetic and plastic gene expression responses to climate change in a key alpine forest tree species

Zhiqin Long[1#], Yupeng Sang[1#], Jiajun Feng[1#], Xinxin Zhang[1], Tingting Shi[1], Lushui Zhang[2], Kangshan Mao[1], Loren H. Rieseberg[3], Jianquan Liu[1], Jing Wang[1*]

1 Key Laboratory of Bio-Resource and Eco-Environment of Ministry of Education, College of Life Sciences, Sichuan University, Chengdu, Sichuan, China

2 Ecological Security and Protection Key Laboratory of Sichuan Province, Mianyang Normal University, Mianyang, Sichuan, China

3. Department of Botany and Biodiversity Research Centre, University of British Columbia, Vancouver, British Columbia, Canada

# These authors contributed equally

* Corresponding author: wangjing2019@scu.edu.cn

ABSTRACT

Despite widespread biodiversity loss, our understanding of how species and populations will respond to accelerated climate change remains limited. In this study, we predict the evolutionary responses of *Populus lasiocarpa*, a key alpine forest tree species primarily found in the mountainous regions of a global biodiversity hotspot, to climate change. We accomplish this by generating and integrating a new reference genome for *P. lasiocarpa*, re-sequencing data for 200 samples, and gene expression profiles for leaf and root tissue following exposure to heat and waterlogging. Analyses of the re-sequencing data indicate that demographic dynamics, divergent selection, and long-term balancing selection have shaped and maintained genetic variation within and between populations over historical timescales. In examining genomic signatures of contemporary climate adaptation, we found that haplotype blocks, characterized by inversion polymorphisms that suppress recombination, play a crucial role in clustering environmentally adaptive variations. Comparison of evolved and plastic gene expression show that genes with expression plasticity generally align with evolved responses, highlighting the adaptive role of plasticity. Lastly, we incorporated local adaptation, migration, genetic load, and plasticity responses into our predictions of population-level climate change risks. Our findings reveal that western populations, primarily distributed in the Hengduan Mountains—a region known for its environmental heterogeneity and significant biodiversity—are the most vulnerable to climate change and should be prioritized for conservation and management. Overall, our study advances understanding of the relative roles of long-term natural selection, local environmental adaptation, and immediate plasticity responses in driving evolutionary adaptation to climate change in keystone species.

INTRODUCTION

Environmental changes driven by ongoing anthropogenic climate change have led to shifts in species ranges, population decline, and even extinction, establishing it as a significant driver of global biodiversity loss. In this context, a critical priority for biodiversity conservation is understanding and monitoring how keystone species in the local ecosystem respond to rapid climate change [1]. Genomic data serves as one of the primary repositories for recording genetic adaptation to past environmental fluctuations and offers a potential useful tool for predicting the evolutionary potential for future adaptation in the context of climate change [2]. Integration of ecological and climate genomics is needed to better comprehend and forecast the impacts of climate change on diversity at the genome, population, and species levels [3].

In the face of unprecedented environmental changes, natural populations-particularly plants with limited mobility-can persist *in situ* through genetically based evolutionary changes and/or environmentally induced phenotypic and gene expression plasticity. Alternatively, they may face the risk of extirpation. In the context of genetically adaptive evolution, various evolutionary processes, including mutation, natural selection, and recombination, play pivotal roles in shaping responses to climate change [4]. The ability to rapidly respond to environmental changes largely depends on the amount of standing adaptive genetic variation, including adaptive single nucleotide polymorphisms (SNPs), short insertions/deletions (indels), and large structural variants (SVs). These variants are largely maintained by long-term balancing selection and/or divergent selection within and among populations [5]. Notably, one type of SV, inversion polymorphisms, has been repeatedly linked to local ecological adaptation in species such as mimetic butterflies [6], monkey flowers [7], sunflowers [8], and deer mouse [9]. Inversions suppress recombination in heterozygotes, helping to keep cassettes of locally adapted alleles together in the face of maladaptive gene flow.

In addition, gene expression variation is highly sensitive to environmental effects, and thus environmentally induced expression plasticity is hypothesized to be crucial for facilitating an immediate response to rapid environmental change [10]. However, the

relationship between evolutionary adaptation and environmental plasticity remains poorly understood. For instance, plastic changes can be adaptive if the direction of plastic response aligns with the direction of natural selection, serving as a steppingstone to reach a fitness optimum in the new environment. Conversely, plasticity is maladaptive if the direction of plastic responses is opposite to the direction of evolved response, potentially moving individuals further away from the fitness optimum [10-13]. Therefore, elucidating the relative roles of evolutionary genetic adaptation, immediate plastic expression changes, and their interactive roles for organismal adaptation to new environments is crucial for a comprehensive understanding of the mechanisms driving adaptation, vulnerability, and resilience during the responses of natural populations to future climate change.

Forest ecosystems serve as habitats for biodiversity and provide environmentally friendly products for humans. Functioning as architects of ecosystems, trees efficiently act as carbon sinks, playing a crucial role in the global carbon cycle [14]. However, due to their lengthy lifespans, most trees face significant challenges in keeping up with rapid climate change, particularly considering that the threat is likely to manifest within the lifetime of a single individual [15, 16]. The mountains of Southeast Asia, with their highly complex and heterogeneous environments, are recognized as global biodiversity hotspots, notable for exceptional species endemism [17]. Given the increasing environmental fluctuations, species in this region are particularly vulnerable to maladaptation under future climate change risks [18]. *Populus lasiocarpa*, a dominant and endemic dioecious tree species, is distinguished by its large leaves within the genus *Populus* and is primarily distributed in mountain regions surrounding the Sichuan Basin in Southeast Asia [19]. Natural populations are found in the Hengduan Mountains (west), Qinling Mountains (north), Daba and Wushan Mountains (east), and Yunnan-Guizhou Plateau (south) (Fig. 2A). This ring-shaped distribution makes *P. lasiocarpa* an ideal system for exploring the evolutionary forces and genetic mechanisms underlying climate adaptation and stress tolerance in natural forest populations in these mountainous regions [20, 21]. There is a pressing need for comprehensive prediction and assessment of a species' population-level vulnerability to future climate change,

102 particularly for keystone forest trees endemic to this area.

103 In this study, we constructed a *de-novo* chromosome-level reference genome of *P.*
104 *lasiocarpa* and subsequently acquired whole-genome re-sequencing data from 200
105 individuals representing 22 populations across its natural distribution range (Fig. 2A;
106 Supplementary Fig. 1). Additionally, we obtained RNA-seq data for experimental
107 seedlings from western and eastern populations, reflecting adaptation to distinct
108 thermal and waterlogging environments under both control and stress conditions in leaf
109 and root tissues. With this comprehensive genomic and transcriptomic dataset, our
110 objectives are as follows: (1) investigate how demographic histories, geography, and
111 natural selection have influenced the patterns of genomic variation; (2) dissect the
112 genetic basis and identify potential adaptive variants facilitating local environmental
113 adaptation; (3) examine the relative roles and intricate relationships between
114 genetically-based evolutionary changes and environmentally-induced expression
115 plasticity underpinning responses to changing environments; (4) predict the future
116 vulnerability of populations to climate change, and identify those populations at the
117 highest risk and that require urgent management actions.
118

119 **RESULTS**

120 **High-quality reference genome assembly of *P. lasiocarpa***

121 A multifaceted sequencing approach, including 49.95 Gb of Nanopore sequencing
122 reads (~119x), 36.37 Gb of Illumina reads (~87x), and 62.52 Gb of high-throughput
123 chromosome conformation capture (Hi-C) reads (~149x), was used for chromosome-
124 scale genome assembly of *P. lasiocarpa* (Supplementary Tables 1). After initial genome
125 assembly, multiple rounds of polishing and redundant sequences filtering
126 (Supplementary Table 2), the final assembly captured 419.54 Mb of genome sequences,
127 with a contig N50 size of 9.19 Mb and 99.23% of the assembled sequences anchored
128 to 19 pseudo-chromosomes (Supplementary Fig. 2; Supplementary Table 3). The
129 completeness and accuracy of the assembled genome were validated and supported by

130 a high proportion (97.9% and 97.8%, respectively) of recalled single-copy orthologs
131 from the Benchmarking Universal Single-Copy Orthologs (BUSCO)[22] and Illumina
132 short reads mapping rate (Supplementary Tables 4,5).

133 We subsequently annotated repetitive elements, protein-coding genes and non-
134 coding RNAs. In total, transposable elements (TEs) made up 40.2% of the genome,
135 with retrotransposons and DNA transposons representing 20.8% and 15.9% of the
136 genome, respectively (Supplementary Table 6). After using a comprehensive strategy
137 combining homology-, transcriptome- and *ab initio*-based prediction, a total of 39,008
138 protein-coding genes were annotated with high confidence (Figure 1; Supplementary
139 Tables 7,8). Among the predicted protein-coding genes, 93.96% could be annotated
140 through at least one of the public protein-related databases (Pfam, NR, InterPro, KEGG,
141 Swiss-Prot, KOG, COG, TrEMBL and GO) (Supplementary Table 9). In addition, we
142 predicted 5,322 non-coding RNAs containing ribosomal RNAs, transfer RNAs,
143 microRNAs, and small nuclear RNAs (Supplementary Table 10).

144

145 **Population genetic analyses offer insights into evolutionary history**

146 To examine the relationships and divergence among populations of *P. lasiocarpa,*
147 we conducted re-sequencing of 200 accessions from 22 populations spanning its natural
148 distribution in Southwest China (Fig. 2A1). The sequencing was performed at an
149 average depth of approximately 25×, with a mapping coverage of 95% (Supplementary
150 Table 11). Following a series of rigorous filtering steps (see Methods), we identified a
151 total of 10,567,146 high-quality SNPs, 1,534,259 indels, and 64,954 SVs. To validate
152 the quality of SVs detected in this study, we inferred population structure using a
153 randomly sampled set of 156,324 linkage disequilibrium (LD)-pruned SNPs and 9,989
154 SVs. Both datasets exhibited highly consistent results (Fig. 2A2; Supplementary Fig.
155 3).

156 Both neighbor-joining (NJ) phylogenetic tree and principal component analysis
157 (PCA) unveiled the presence of four genetic clusters within *P. lasiocarpa* corresponding
158 to the West, East, Southwest, and Hybrid groups (Fig. 2A2). The West group consists

of 70 individuals from eight populations primarily distributed in the Hengduan Mountains in western areas of the Sichuan Basin. The East group encompasses 110 individuals from 12 populations distributed in the Daba and Wushan Mountains in eastern areas of the Sichuan Basin. In contrast to the two main groups of western and eastern populations, the Southwest and Hybrid groups only include 10 individuals separately. Additionally, clustering analysis conducted by ADMIXTURE identified the strongest support for K=3 populations, thereby supporting the separation of West, East, and Southwest groups of populations (Fig. 2A2). Due to the high level of inter-population admixture in the Hybrid group, we subsequently excluded this group from the following analysis.

To delve further into divergence and demographic histories, we initially employed TreeMix to infer the phylogenetic tree topology among the three main groups. The results indicated that the Southwest and West groups shared a recent common ancestor, with a migration edge suggesting gene flow from East to Southwest group (Fig. 2B1). Another haplotype sharing analysis revealed that individuals within the same group exhibited more and longer identity-by-descent blocks compared to those from different groups. Notably, there was a lower and shorter haplotype-sharing pattern observed between the West and East groups than between each of them and the Southwest group (Fig. 2B2).

Subsequently we applied the pairwise sequentially Markovian coalescent (PSMC) model to infer the fluctuations in effective population size (N_e) over time in each group. The results supported a shared decline of populations among these groups (Fig. 2B3). Recognizing the limited power of recent N_e trajectory inference for PSMC, we employed SMC++ to explore the more recent demographic history of these populations. Compared to the continuous reduction in N_e observed in the Southwest group, both the West and East groups experienced recent population expansion following a shared bottleneck after the Last Glacial Maximum (Supplementary Fig. 4). We further estimated the divergence time between the population groups, revealing that the West group diverged from the East group approximately 66 thousand years ago (Kya). The subsequent divergence time between the Southwest and West group was estimated at

189 approximately 47 Kya (Fig. 2B4).

190 Furthermore, we investigated and compared patterns and levels of nucleotide
191 diversity (π) and genetic differentiation (F_{ST} and d_{XY}) among the populations. Consistent
192 with the slower rate of LD decay observed in the Southwest group of populations
193 (Supplementary Fig. 5), nucleotide diversity was also found to be lowest (π=4.59×10^{-}
194 ^{3}) compared to the West (π=5.67×10^{-3}) and East (π=5.12×10^{-3}) groups of populations
195 (Fig. 2B5), aligning with the corresponding bottleneck observed in this group. Finally,
196 after adjusting for the varying number of individuals in each group, we randomly
197 selected 10 individuals from the three groups and obtained highly consistent results in
198 the analysis of π, LD, F_{ST}, d_{XY} and recent demographic history (Supplementary Fig. 6).
199

200 **Genome-wide signatures of divergent and balancing selection**

201 Ancient polymorphisms may be sustained through long-term balancing selection during
202 population divergence, resulting in genomic regions with increased genetic diversity
203 within and among nascent populations[23]. Alternatively, ancestral balanced
204 polymorphisms might be sorted unequally across descendant lineages by selection and
205 drift, leading to genomic regions with increased divergence [24, 25]. These
206 evolutionary forces can give rise to genomic regions with heterogeneous patterns of
207 relatedness, potentially confounding overall population structure. To unveil the
208 evolutionary processes shaping the landscape of genomic divergence, we initially
209 excluded the Southwest group, given its smaller individual size compared to the other
210 two main groups. We then characterized local population structure by estimating
211 multidimensional scaling (MDS) in non-overlapping windows of 250 SNPs along the
212 genome using a local PCA approach [26]. To identify outlier windows, we selected the
213 top and bottom 0.5% windows in the MDS1 (Fig. 3A). In comparison with the genomic
214 background windows, the two extreme windows exhibited distinct phylogenetic
215 clustering topologies and population-wide relationships (Fig. 3B), suggesting that these
216 regions are likely under long-term balancing selection (the top 0.5% windows) and
217 divergent selection (the bottom 0.5% windows) respectively.

To further explore the potential evolutionary processes driving the divergent patterns of genomic variation in these regions, we compared the level of nucleotide diversity (π), Tajima's D, both the relative (F_{ST}) and absolute (d_{XY}) genetic divergence, and the cross-population composite likelihood ratio statistics (XP-CLR) among the three types of windows. Consistent with the hypothesis of long-term balancing selection, we found that the top 0.5% windows showed significantly elevated π, more positive values of Tajima's D, higher d_{XY}, and lower F_{ST} and XP-CLR values compared to genomic background windows. Consequently, we referred these windows as 'Balancing selection (BLS) regions' (185 BLS windows with a total length of 1.32 Mb; ~0.32% of the assembled genome) (Fig. 3 and Supplementary Table 12). Further Gene Ontology (GO) functional enrichment analysis of the 166 candidate genes in BLS regions revealed categories significantly enriched in the metabolic process and biotic stress response, including thiamine, oxazoline and thiazoline metabolic and biosynthetic processes that play a crucial role in responding to DNA damage and pathogen attack in plants (Supplementary Fig. 7B). Specifically, multiple genes under balancing selection were orthologous to *Arabidopsis* genes associated with plant immune responses (Supplementary Fig. 8). For example, *Polas33741* (Fig. 3D1) was orthologous to *WRKY72*, which was found to regulate defense-related and jasmonic acid (JA) biosynthesis genes in many plants [27].

Conversely, we found that the bottom 0.5% windows exhibited strongly decreased π, more negative values of Tajima's D, higher d_{XY}, higher F_{ST}, and XP-CLR compared to background windows and were henceforth referred to as 'Divergent selection (DS)' regions (185 DS windows with a total length of 1.76 Mb; ~0.42% of the assembled genome) (Fig. 3 and Supplementary Table 13). GO enrichment analyses of 163 candidate genes in DS regions were significantly enriched in biological processes of xenobiotic stimulus and oxidative stress responses (Supplementary Fig. 7A). Specifically, many genes that showed high divergence and positive selection signatures were functionally related to organ development, rhythm control, and hypoxia adaptation (Supplementary Fig. 7C; Supplementary Fig. 9; Supplementary Table 13). For example, *Polas12612* (Fig. 3D2), the ortholog in *Arabidopsis* (*CKX5*) was found

248 to be the downstream target gene of the phytochrome-interacting factor 4 (*PIF4*), which
249 regulates photoperiod-dependent morphogenesis [28]; *Polas20885*, the ortholog (*TIC*)
250 of which is involved in circadian rhythms control of plant [29]. Therefore, these
251 candidate genes within the divergent selection regions likely underlie divergent
252 ecological adaptation to the disparate mountain environments between the West and
253 East lineages of *P. lasiocarpa*.

254

255 **The genomic signatures of environmental adaptation**

256

257 To identify genomic variants associated with various environmental variables, we
258 combined the Latent Factor Mixed Model (LFMM) [30] and Genome-wide Efficient
259 Mixed Model Association (GEMMA) [31] to test the association between variant
260 genotypes and each of the 29 environmental variables, while accounting for the
261 confounding effects of population structure. We identify a total of 19,955 putatively
262 adaptive variants from the overlapping results of LFMM and GEMMA (Supplementary
263 Table 14), which are distributed widely across the genome (Supplementary Fig. 10).
264 These variants include not only SNPs and short Indels (Supplementary Fig. 11) but also
265 SVs, which are often overlooked (Supplementary Fig. 12). A functional enrichment
266 analysis of the 2,044 genes with variants associated with environmental adaptation
267 revealed significant enrichment in GO categories related to catabolic and metabolic
268 processes (Supplementary Table 15), which are crucial for the survival of plants facing
269 environmental changes [32, 33].

270 To further assess the robustness of the locally adaptive variants identified, we
271 initially employed Mantel and partial Mantel tests to evaluate patterns of isolation-by-
272 distance (IBD) and isolation-by-environment (IBE) for the environmental-associated
273 "adaptive" variants and randomly selected "neutral" variants. Our results revealed that
274 both adaptive and neutral variants exhibited strong patterns of IBD. However, after
275 accounting for geographic effects with a partial Mantel test, we observed a significant
276 correlation between pairwise genetic distance between populations (F_{ST}/1-F_{ST}) and

environmental distance for adaptive variants. This was in contrast to the weak pattern of IBE observed in neutral variants (Supplementary Fig. 13). This suggest that the adaptive variants are primarily influenced by environmental gradients rather than neutral factors like population structure and geographic distance. Additionally, we employed a machine learning algorithms, gradient forest, to compare the shape of allele frequency turnover along the environmental gradient for adaptive and neutral variants from random sampling. Our findings indicated that the cumulative importance of allele frequency changes in the adaptive variants differed in shape and magnitude from those in the neutral reference datasets, suggesting that environmental variation more effectively explains allele frequency changes in the local adaptive variants compared to the reference variants (Supplementary Fig. 11D; Supplementary Fig. 12E).

Haploblocks facilitates local adaptation

Large haploblocks, especially inversions, have been implicated to play a key role in local adaptation, primarily by facilitating the capture and linkage of multiple locally adaptive alleles through the suppression of recombination within co-inherited haplotype blocks [34-36]. Recent advancements in population genomic approaches have proven to be powerful and effective in detecting potential inverted regions across a diverse range of species [26]. In this study, we used an unbiased genome-wide scan approach with local principal component analyses (PCA) to characterize population structure and identify outlier regions using windows of 60 SNPs in size throughout the genome in *P. lasiocarpa.* To pinpoint putative inverted regions, we focused on genomic regions where individuals were distinctly clustered into three groups corresponding to the three possible inversion genotypes on the first principal component. The center cluster, showing the highest heterozygosity, was consistent with inversion heterozygotes (see Methods). We identified a total of 218 haploblocks, ranging in size from 10 to 650 kbp and encompassing 647 genes. GO categories within these haploblocks were notably enriched in ethylene-activated and phosphorelay signal

transduction and signaling pathways (Supplementary Table 16).

To further substantiate the association of these haploblocks with structural variations, particularly inversions, we analyzed population-scale recombination rates, deleterious mutation loads (the ratio of zero-fold to four-fold variants), genetic divergence between populations (F_{ST}), and overall nucleotide diversity (π) in comparison to randomly sampled genomic regions of the same size (Fig. 4A). Firstly, consistent with inversion polymorphisms that suppress recombination between haplotypes, the haploblock regions exhibited significantly lower recombination rates compared to the randomly sampled genomic regions. Secondly, these haploblock regions had a higher deleterious mutation load relative to the rest of the genome, consistent with heightened Hill-Robertson interference in inverted regions due to the suppression of recombination [37]. Lastly, the haploblock regions demonstrated significantly higher nucleotide diversity and genetic differentiation across populations compared to other genomic regions, further supporting the 'local adaptation hypothesis' [34-36]. Overall, while the haploblocks identified here show inversion-like characteristics, further independent evidence, such as long-read sequencing and comparative genetic mapping, is needed for additional confirmation.

To further investigate the role of these haploblocks in the local environmental adaptation of *P. lasiocarpa*, we compared the number of environmental adaptive variants within the haploblock regions to those in randomly sampled reference regions of the same size. Our analysis revealed a notable presence of 1,862 putatively adaptive variants in the haploblock regions, significantly exceeding expectations (Fig. 4A). This strongly suggest that these haploblocks, particularly the putative inversion polymorphisms, constitute a crucial source of genetic variation that facilitates local population differentiation and environmental adaptation [8, 38]. For instance, a haploblock on chromosome 9, spanning 44,913bp, contained 508 adaptive variants (447 SNPs, 60 Indels, and one SV), which were strongly associated with Precipitation of Coldest Quarter (BIO19) (Fig. 4B). This haploblock is characterized by high LD, and PCA revealed three distinct genotype clusters within the region, with higher heterozygosity in the central cluster. This pattern aligns with the expectation of

inversion polymorphism, where the two extreme clusters represent homozygous genotypes for two distinct haplotypes, and the central cluster represents heterozygotes (Fig. 4B). Notably, four genes were identified in this region, including *Polas22852*, orthologous to *Arabidopsis AGP31*, known to be involved in vascular tissue function during defense responses, including responses to Methyl jasmonate and abscisic acid (ABA) treatments [39]. Another noteworthy example is a putative adaptive inversion spanning 21,893bp, which trapped 43 Temperature Seasonality (BIO4)-associated variants (38 SNPs, 4 Indels, and one SV) (Fig. 4C). Three genes were located within this region, including *Polas23357*, the ortholog of which (*RLP27*) was found to be involved in signal transduction and defense responses [40].

The role of environmentally induced gene expression plasticity in rapid climatic adaptation

In addition to genetic changes susceptible to selection, we also explored the potential role of immediate plastic responses to environmental shifts. This approach is crucial for understanding whether phenotypic plasticity can lead to subsequent genetic adaptations. Since gene expression changes are highly responsive to environmental fluctuations and often serve as a link between the genome and the phenotype, we focused on gene expression levels as primary traits. Our aim is to clarify how the interaction between expression plasticity and evolutionary adaptation shapes rapid responses to environmental change [10-12]. To achieve this, we analyzed gene expression differences under both controlled and stress-inducing conditions (heat and waterlogging) for plants sampled from two populations with distinct temperature and precipitation-related environments (Figure 5A). These two populations were designed as West and East ecotypes for the downstream analysis.

We performed transcriptome sequencing on leaf and root tissues from both East and West ecotypes under two conditions: control and stress (heat and waterlogging), to simulate anticipated future environmental changes (Fig. 5A). Initial analysis using

365 hierarchical clustering of expression profiles revealed that leaf and root tissue samples
366 clustered into two distinct groups (Supplementary Fig. 14A). This finding was
367 confirmed by principal component analysis (PCA), where PC1, accounting for 41.85%
368 of the variance, reflected tissue-specific differences, and PC2, accounting for 12.92%
369 of the variance, represented distinctions related to treatment types (Supplementary Fig.
370 14B). To further explore and compare the transcriptional responses of the two ecotypes
371 to environmental stresses, we conducted pairwise contrasts between treatments within
372 each ecotype (Supplementary Fig. 15A). We found that approximately 14% to 45% of
373 the differentially expressed genes were shared between ecotypes, with variation
374 depending on the environmental conditions (Supplementary Fig. 15B). Differentially
375 expressed genes between treatments were enriched for GO terms associated with heat
376 and water stress responses, respectively (Supplementary Fig. 15C).

377 To further investigate and characterize the relationship between plastic and evolved
378 transcriptional responses to environmental changes, we compared the stress-induced
379 gene expression plasticity in the West ecotype with the evolved expression differences
380 between the West and East ecotypes (Supplementary Fig. 16A2, B2). The rationale
381 behind this comparison assumes that the West ecotype represents the population akin
382 to the "ancestral" state, whereas the East ecotype is perceived to be closer to the
383 "evolved" state as it more closely aligns with and adapts to changing environments
384 characterized by higher temperature and precipitation (Supplementary Fig. 16A1, B1).
385 Therefore, if gene expression plasticity is adaptive, we would expect the direction of
386 plastic responses to align with the direction of evolved responses. Conversely, if
387 plasticity is maladaptive, we would anticipate that plastic responses would oppose
388 evolved responses (Supplementary Fig. 16A3, B3).

389 We identified 1,078 genes whose expression significantly diverged between the
390 West and East ecotypes under control conditions in leaf tissues (FDR<0.05). Among
391 these, 259 genes exhibited heat-induced plastic responses in the same direction as
392 evolved responses, while 154 genes showed oppositing expression directions (Fig.
393 5B1). Furthermore, there was a strong positive correlation between plasticity and
394 evolved divergence (Spearman's $\rho = 0.33$, Fig. 5B1, inset). To account for potential

395 statistical artifacts from regression toward the mean, we conducted a randomization test
396 to estimate a null distribution of correlation coefficients. This test confirmed that the
397 observed correlation was significantly more positive than would be expected by chance
398 alone (binomial exact tests $P < 0.01$, Fig. 5B1, inset). These results suggest that many
399 of the expression responses to heat stress are adaptive, supporting the idea that adaptive
400 plasticity contributes to local environmental adaptation. In root tissues, gene expression
401 profiles showed a similar pattern, with significantly more adaptive plasticity under heat
402 stress (Spearman's $\rho = 0.82$, Fig. 5B2). Additionally, expression correlation coefficients
403 between waterlogging-induced plasticity and evolution were 0.36 for leaf and 0.76 for
404 root tissues, respectively (Fig. 5C1; Fig. 5C2), further reinforcing the pattern that plastic
405 expression responses align with evolved responses.

406 Among the 4,507 genes displaying heat-induced adaptive plasticity (259 in leaf
407 and 4,330 in root tissues), we observed a significant enrichment in genes associated
408 with genetic adaptation to local environments, as previously identified (Fig. 5B3). This
409 supports the role of selection on adaptive gene expression plasticity. GO enrichment
410 analysis further revealed that these adaptive plasticity genes were significantly enriched
411 in terms related to stress and defense responses, such as "regulation of response to
412 stress", "defense response", and "response to abiotic stimulus" (Fig. 5B4). Notably
413 examples include *Polas12092*, which is orthologous to *Arabidopsis ILL6* and involved
414 in the jasmonic acid signaling pathway in response to abiotic stress [41]; *Polas02648*,
415 orthologous to *SMXL7*, a negative regulator of drought resistance through regulation of
416 the strigolactone signaling pathways [42]; and *Polas06886*, orthologous to *WRKY11*,
417 which plays crucial roles in heat and drought tolerance in rice and *Arabidopsis* [43]
418 (Supplementary Fig. 17A).

419 Similarly, among the 3,812 genes showing waterlogging-induced adaptive plastic
420 responses (115 genes in leaf and 3,719 genes in root tissues), we also observed
421 significant enrichment of genes associated with genetic adaptation (Fig. 5C3),
422 reinforcing the role of selection on these gene sets. GO analysis indicated that genes
423 with putatively adaptive plasticity were enriched in terms related to "regulation of
424 response to alcohol," "response to hypoxia," "response to abscisic acid," and "response

425 to jasmonic acid," highlighting their importance in waterlogging stress responses (Fig.
426 5C4). For example, several genes from key hormone- and stress-responsive
427 transcription factor families (i.e. WRKY, ERF, and DOF), including orthologs of *CDF2*,
428 *ERF1* and *WRKY40* (Supplementary Fig. 17B), are critical for plant survival and
429 reproduction under various biotic and abiotic stresses [44, 45].

430

431 **Evolutionary genomic prediction of population-level vulnerability to future**
432 **climate change**

433

434 Accelerated climate change is profoundly posing a threat to global and local
435 biodiversity, especially in mountainous areas that harbour exceptional endemism and
436 species richness. The mountain regions around Sichuan Basin have experienced
437 repeated and drastic climatic oscillation [46]. Consequently, our study offers a valuable
438 opportunity to enhance our understanding of species' response to future climate change
439 in this crucial region. To explore the landscape of adaptive variation, we calculated an
440 adaptive index, which estimates genetic similarities and differences based on the
441 redundancy analysis (RDA), and mapped it across the geographic distribution of *P.*
442 *lasiocarpa* [47]. After adjusting for correlations among environmental variables, we
443 conducted RDA using the remaining seven environmental variables as predictors. This
444 analysis revealed that most of the adaptive variation is concentrated along RDA1,
445 which explains 78.83% of the variance. Extrapolating the adaptive gradients associated
446 with RDA1 onto the landscape revealed a striking contrast in the adaptation index:
447 eastern areas are characterized by warmer annual temperatures and higher precipitation
448 during the warmest quarter (positive RDA1 scores), while western areas exhibit a
449 strong shift in precipitation seasonality (negative RDA1 scores) (Fig. 6A).

450 Next, we investigate the capacity and vulnerability of natural populations to future
451 climate change, aiming to predict which populations or regions might face the highest
452 risks. To accomplish this, we utilized the Gradient Forest (GF) approach to quantify
453 genomic offset, which assess the extent of genetic change required for a population to
454 keep pace with future environmental conditions by modeling the turnover of adaptive

genetic composition in response to projected future climates [48]. In addition to calculate local genetic offset, which assumes *in situ* tolerance, we further estimated two other metrics- forward and reverse genetic offsets- to assess the maladaptation of populations when simultaneously considering the contributions of *in situ* adaptation and migration to future shifting climates. Forward genetic offset calculates the minimum predicted offset, assuming populations could move (or be relocated) anywhere in Eurasia, while reverse genetic offset calculates the minimum offset between hypothetical populations in future climates and current populations within the existing range.

To measure the genetic changes needed for adaptation to new climate conditions across populations at various time points, we integrated projections from three different future climate models (CMCC-ESM2, GISS-E2-1-G, MPI-ESM1-2-HR) under moderate (SSP245) and severe (SSP585) shared socioeconomic pathways for the years 2080 (2061-2080) and 2100 (2081-2100), accounting for variability between climate models. The estimates of local, forward, and reverse offsets across different models showed highly consistent results (Supplementary Fig. 18), showing that populations in western areas exhibited greater genetic offset than those inhabiting eastern regions of the distribution ranges. Additionally, the spatial patterns of genomic offset align closely whether using all 19 climate variables or the seven uncorrelated variables identified from RDA analyses (Supplementary Fig. 19). Therefore, in the main text, we present the results averaged from the three climate models using all 19 climatic variables under the moderate scenario (SSP245) for the 2060-2080 period (Figure 6B). Again, the predicted patterns of substantially higher local, forward, and reverse offsets suggest that western populations distributed in the Hengduan Mountains are likely to be particularly vulnerable under future climates, as neither in situ adaptation nor migration are likely to be effective at reducing the population-level vulnerability to climate change in this region.

Finally, to further assess whether vulnerable western populations have already been adversely affected by recent unfavorable climate conditions, we measured genomic load. Deleterious genetic variants are expected to be less efficiently purged by purifying

485 selection in populations already in decline coinciding with shifts in climate [49]. The
486 genomic load for each population was estimated by calculating the proportion of
487 derived loss-of-function (LoF) and deleterious variants relative to synonymous ones.
488 Our findings reveal that the load of LoF variants did not show significant differences
489 between western and eastern populations, implying that selection in both groups is
490 effective at purging severely deleterious mutations. However, we observed a significant
491 positive relationship between the ratio of deleterious to synonymous variants and the
492 predicted local genomic offset across the sampled populations (Figure 6C). Western
493 populations exhibited significantly higher loads of deleterious mutations compared to
494 eastern populations, indicating that these populations may already be threatened by
495 ongoing climate change. This shift has likely impacted the efficacy of removing
496 moderately deleterious variants, contributing to detrimental effects in these regions.
497

498 **Discussion**

499

500 Global climate change is increasingly exacerbating biodiversity loss. To better
501 understand and predict species' responses and dynamics in the face of climate change,
502 it is essential to adopt an evolutionary perspective that incorporates both genetic and
503 plastic effects [50]. Forecasts of future evolutionary responses to ongoing and future
504 climate change rely heavily on the investigation of historical and contemporary
505 adaptive evolutionary responses [3, 51]. In mountainous regions, highly heterogeneous
506 environments and physical barriers often drive intraspecific genetic differentiation and
507 local ecological adaptation in species [46]. Here we highlight the unique value of
508 integrating evolutionary genomic approaches to predict and monitor species and
509 population responses to global climate change, using *P. lasiocarpa*, an endemic and
510 dominant tree species distributed in the biodiversity hotspot of the mountain regions of
511 Southeast Asia. By leveraging a newly assembled high-quality reference genome and
512 population genomic datasets, we explore the processes of adaptive evolution in

513 response to climate change across historical, contemporary, and future timescales
514 (Figure 7).

515 Our results first revealed a clear genetic separation between western and eastern
516 populations, with the Sichuan Basin acting as both a geographical and genetic barrier,
517 leading to a ring diversification pattern in *P. lasiocarpa*. Both lineages exhibited
518 consistent demographic histories, suggesting that the climatic oscillations of the
519 Quaternary similarly impacted both groups. Beyond neutral evolutionary processes like
520 genetic drift and demographic changes, our findings demonstrated that genomic
521 diversity and divergence were significantly shaped by divergent selection and long-
522 term balancing selection. Regions under divergent selection, marked by strong
523 signatures of positive selection in both lineages, exhibited higher levels of relative and
524 absolute genetic divergence (F_{ST} and d_{XY}) across populations and displayed a
525 phylogenetic topology that clearly separated western and eastern lineages. Genes in
526 these regions were enriched in categories related to environmental stimuli and stress
527 responses, underscoring their crucial roles in driving differential adaptation to local
528 climates in the two independent lineages [52]. Conversely, we identified regions with
529 remarkable genetic diversity and elevated levels of trans-lineage shared polymorphism,
530 likely maintained by long-term balancing selection [23]. These regions were
531 significantly enriched for genes involved in metabolic processes and responses to biotic
532 stresses. Together, these findings highlight the significant roles of divergent and long-
533 term balancing selection, alongside historical demographic processes, in shaping the
534 standing genetic variation to keep pace with climate change.

535 Identifying climate-associated adaptive genetic variation and characterizing its
536 spatial distribution patterns can provide valuable insights into the adaptive potential of
537 populations facing changing climates [2]. Our findings reveal numerous polymorphic
538 haploblocks, characterized by features consistent with inversions, which significantly
539 enrich locally climate-adaptive variants. Consistent with recent studies in sunflowers
540 [8], deer mice [9], and an invasive weed species [53], our results suggest that
541 haploblock polymorphisms may play a crucial role in maintaining the genetic basis of
542 local adaptation. This is particularly important as the suppression of recombination

543 within these regions can protect locally advantageous allele combinations from being
544 diluted by migration, especially in the context of high gene flow [38]. However, we
545 cannot yet determine whether the haploblocks detected here are associated with
546 inversions or are closely linked alleles experiencing low recombination. Future research
547 involving population-level long-read sequencing and molecular experiments is needed
548 to better characterize these haploblocks. Additionally, we found that haploblock regions
549 tend to accumulate deleterious mutations, likely due to the reduced efficacy of purifying
550 selection caused by suppressed recombination [37]. This raises the unresolved question
551 of the trade-off between the benefits of concentrating climate-adaptive variations and
552 the costs of accumulating deleterious mutations within haploblocks. Addressing this
553 paradox will require further research.

554 In addition to genetic responses to climate change, molecular phenotypic plasticity
555 offers an immediate buffer against its negative effects. Our findings reveal that plastic
556 gene expression changes generally align with evolved responses, indicating the
557 predominance of adaptive plasticity to environmental stresses, as observed in multiple
558 other systems [12, 54, 55]. Initial adaptive plasticity may serve as a critical stepping
559 stone for populations to survive and persist under changing and novel environmental
560 conditions. This short-term acclimation response can create more opportunities for
561 natural selection to act, ultimately facilitating long-term adaptive evolution [56]. This
562 process may be particularly important for rapid, within-generation responses to climate
563 change in long-lived trees [57]. Indeed, we found that genes exhibiting adaptive
564 expression plasticity show significant enrichment for climate-adaptive genetic variation,
565 suggesting that genetic changes may have occurred in these genes. This might be
566 because these populations have frequently encountered stressful environmental
567 conditions, leading to gene expression plasticity being partly shaped to be adaptive
568 under recurrent selective pressures, potentially resulting in genetic assimilation [58].

569 Finally, exploring and understanding the evolutionary forces and genomic
570 architecture underlying contemporary climate adaptation provide a crucial baseline for
571 forecasting species' responses to ongoing and future climate change [2, 4]. By
572 considering intraspecific adaptive variation and the mitigating effects of migration, our

findings indicate that western populations are likely to be particularly vulnerable to future climate change, exhibiting higher local, forward, and reverse genomic offsets compared to eastern populations. Additionally, we found that western populations carry a greater genetic load of mildly deleterious mutations than eastern populations. While other factors affecting the demography of western populations cannot be ruled out, our results indicate that past and ongoing climate change may have intensified the decline of these populations, weakening purifying selection and reducing their fitness in changing environments. Furthermore, given the prominent role of adaptive gene expression plasticity in western populations, it remains uncertain whether this adaptive plasticity will weaken selection intensity, buffer genetic response, or constrain adaptation to altered environmental conditions [13]. Therefore, the interplay between plasticity, genetic variation, selection, and adaptation requires further investigation, particularly in understanding how plastic responses may either facilitate or impede evolutionary responses to climate change.

The western populations are primarily distributed in the Hengduan Mountains, a region known for its highly heterogeneous environments and significant biodiversity, with many endemic mountainous species [17]. Should these key forest tree species become vulnerable to future climate change, it could further jeopardize the local ecosystem and impact the entire endemic flora and fauna of the region. To mitigate local maladaptation, assisted gene flow from eastern to western populations could be an effective strategy, particularly given the natural genetic barrier created by the Sichuan Basin that separates these populations [59]. By introducing favorable genotypes from the eastern populations, which are preadapted to warmer and wetter climates, this approach may enhance the adaptive capacity of western populations to new climatic conditions. However, while our study integrates various evolutionary processes—including demographic histories, selection pressures, local adaptation, gene expression plasticity, and genetic load—to offer a comprehensive understanding of population-level vulnerability to climate change, further carefully designed common garden and transplant experiments are needed [60, 61]. These experiments will help

validate our genomic forecasts and assess the practical benefits and risks of assisted gene flow for effective conservation and management strategies.

Acknowledgements

This work was supported by the National Key Research and Development Program of China (2022YFD2201200). National Natural Science Foundation of China (32371695 and 31971567) and Fundamental Research Funds for the Central Universities (2023SCUNL105) to J.W..

Author contributions

J.W. conceived and supervised the study. Z.L., Y.S., J.F., T.S. analyzed the data. J.F. and X.Z. conducted the stress experiments. K.M. and L.Z. handled the sampling and material collection. Z.L. and J.W. wrote the manuscript, with the input from L.R. and J.L.. All authors approved the final version of the manuscript.

Competing interests

The authors declare no competing interests.

Data availability

All data needed to evaluate the conclusions in the paper are present in the paper and/or the Supplementary Materials. All sequencing data in this study will be deposited in National Genomics Data Center (NGDC) during reviewing process. All scripts used in this study will be available at https://github.com/jingwanglab/Evolutionary-genomics-of-Populus-lasiocarpa upon publication.

References

1. Urban, M. C. et al. Improving the forecast for biodiversity under climate change. *Science* **353**, aad8466 (2016).
2. Bernatchez, L., Ferchaud, A.-L., Berger, C. S., Venney, C. J. & Xuereb, A. Genomics for monitoring and understanding species responses to global climate change. *Nat. Rev. Genet.* **25**, 165-183 (2024).
3. Martin, R. A., da Silva, C. R., Moore, M. P. & Diamond, S. E. When will a changing climate outpace adaptive evolution? *WIRES Clim. Chang.* **14**, e852 (2023).
4. Aguirre-Liguori, J. A., Ramírez-Barahona, S. & Gaut, B. S. The evolutionary genomics of species' responses to climate change. *Nat. Ecol. Evol.* **5**, 1350-1360 (2021).
5. Olson-Manning, C. F., Wagner, M. R. & Mitchell-Olds, T. Adaptive evolution: evaluating empirical support for theoretical predictions. *Nat. Rev. Genet.* **13**, 867-877 (2012).
6. Joron, M. et al. Chromosomal rearrangements maintain a polymorphic supergene controlling butterfly mimicry. *Nature* **477**, 203-206 (2011).
7. Lowry, D. B. & Willis, J. H. A widespread chromosomal inversion polymorphism contributes to a major life-history transition, local adaptation, and reproductive isolation. *PLoS Biol.* **8**, e1000500 (2010).
8. Todesco, M. et al. Massive haplotypes underlie ecotypic differentiation in sunflowers. *Nature* **584**, 602-607 (2020).
9. Harringmeyer, O. S. & Hoekstra, H. E. Chromosomal inversion polymorphisms shape the genomic landscape of deer mice. *Nat. Ecol. Evol.* **6**, 1965-1979 (2022).
10. Swaegers, J. & Koch, E. L. Gene expression studies of plastic and evolutionary responses to global warming. *Curr. Opin. Insect Sci.* **51**, 100918 (2022).
11. Campbell-Staton, S. C., Velotta, J. P. & Winchell, K. M. Selection on adaptive and maladaptive gene expression plasticity during thermal adaptation to urban heat islands. *Nat. Commun.* **12**, 6195 (2021).
12. Josephs, E. B., Van Etten, M. L., Harkess, A., Platts, A. & Baucom, R. S. Adaptive and maladaptive expression plasticity underlying herbicide resistance in an agricultural weed. *Evol. Lett.* **5**, 432-440 (2021).
13. Ghalambor, C. K. et al. Non-adaptive plasticity potentiates rapid adaptive evolution of gene expression in nature. *Nature* **525**, 372-375 (2015).
14. Isabel, N., Holliday, J. A. & Aitken, S. N. Forest genomics: Advancing climate adaptation, forest health, productivity, and conservation. *Evol. Appl.* **13**, 3-10 (2020).
15. Holliday, J. A. et al. Advances in ecological genomics in forest trees and applications to genetic resources conservation and breeding. *Mol. Ecol.* **26**, 706–717 (2017).
16. Browne, L., Wright, J. W., Fitz-Gibbon, S., Gugger, P. F., & Sork, V. L. Adaptational lag to temperature in valley oak (*Quercus lobata*) can be mitigated by genome-informed assisted gene flow. *Proc. Natl Acad. Sci. USA* **116**: 25179-25185 (2019).
17. Myers, N., Mittermeier, R. A., Mittermeier, C. G., Da Fonseca, G. A. & Kent, J. Biodiversity hotspots for conservation priorities. *Nature* **403**, 853-858 (2000).
18. Chen, Y. et al. The combination of genomic offset and niche modelling provides insights into climate change-driven vulnerability. *Nat. Commun.* **13**, 4821 (2022).
19. Li, X., et al. Wind-dispersed seeds blur phylogeographic breaks: the complex evolutionary

history of Populus lasiocarpa around the Sichuan Basin. Plant Divers. **45**: 156-168 (2023).

20. Davis, M. B. & Shaw, R. G. Range shifts and adaptive responses to Quaternary climate change. *Science* **292**, 673-679 (2001).

21. Davis, M. B., Shaw, R. G. & Etterson, J. R. Evolutionary responses to changing climate. *Ecology* **86**, 1704-1714 (2005).

22. Simão, F. A., Waterhouse, R. M., Ioannidis, P., Kriventseva, E. V. & Zdobnov, E. M. BUSCO: assessing genome assembly and annotation completeness with single-copy orthologs. *Bioinformatics* **31**, 3210-3212 (2015).

23. Charlesworth, D. Balancing selection and its effects on sequences in nearby genome regions. *PLoS Genet.* **2**, e64 (2006).

24. Han, F. et al. Gene flow, ancient polymorphism, and ecological adaptation shape the genomic landscape of divergence among Darwin's finches. *Genome Res.* **27**, 1004-1015 (2017).

25. Guerrero, R. F. & Hahn, M. W. Speciation as a sieve for ancestral polymorphism. *Mol. Ecol.* **26**, 5362-5368 (2017).

26. Li, H. & Ralph, P. Local PCA Shows How the Effect of Population Structure Differs Along the Genome. *Genetics* **211**, 289-304 (2019).

27. Bhattarai, K. K., Atamian, H. S., Kaloshian, I. & Eulgem, T. WRKY72-type transcription factors contribute to basal immunity in tomato and Arabidopsis as well as gene-for-gene resistance mediated by the tomato *R* gene *Mi-1*. *Plant J.* **63**, 229-240 (2010).

28. Nomoto, Y., Kubozono, S., Yamashino, T., Nakamichi, N. & Mizuno, T. Circadian Clock- and PIF4-Controlled Plant Growth: A Coincidence Mechanism Directly Integrates a Hormone Signaling Network into the Photoperiodic Control of Plant Architectures in *Arabidopsis thaliana*. *Plant Cell Physiol.* **53**, 1950-1964 (2012).

29. Ding, Z., Millar, A. J., Davis, A. M. & Davis, S. J. TIME FOR COFFEE Encodes a Nuclear Regulator in the *Arabidopsis thaliana* Circadian Clock. *Plant Cell* **19**, 1522-1536 (2007).

30. Frichot, E., Schoville, S. D., Bouchard, G. & François, O. Testing for associations between loci and environmental gradients using latent factor mixed models. *Mol. Bio. Evol.* **30**, 1687-1699 (2013).

31. Zhou, X. & Stephens, M. Genome-wide efficient mixed-model analysis for association studies. *Nat. Genet.* **44**, 821-824 (2012).

32. Vanholme, R., Demedts, B., Morreel, K., Ralph, J. & Boerjan, W. Lignin Biosynthesis and Structure. *Plant Physiol.* **153**, 895-905 (2010).

33. Pascual, M. B. et al. Biosynthesis and Metabolic Fate of Phenylalanine in Conifers. *Front Plant Sci.* **7**, 1030 (2016).

34. Wellenreuther, M. & Bernatchez, L. Eco-Evolutionary Genomics of Chromosomal Inversions. *Trends Ecol. Evol.* **33**, 427-440 (2018).

35. Savolainen, O., Lascoux, M. & Merilä, J. Ecological genomics of local adaptation. *Nat. Rev. Genet.* **14**, 807-820 (2013).

36. Kirkpatrick, M. & Barton, N. Chromosome Inversions, Local Adaptation and Speciation. *Genetics* **173**, 419-434 (2006).

37. McVean, G. A. & Charlesworth, B. The effects of Hill-Robertson interference between weakly selected mutations on patterns of molecular evolution and variation. *Genetics* **155**, 929-944 (2000).

38. Schaal, S. M., Haller, B. C. & Lotterhos, K. E. Inversion invasions: when the genetic basis of

local adaptation is concentrated within inversions in the face of gene flow. *Philos. Trans. R. Soc. Lond. B. Bio. Sci.* **377**, 20210200 (2022).

39. Liu, C. & Mehdy, M. C. A Nonclassical Arabinogalactan Protein Gene Highly Expressed in Vascular Tissues, *AGP31*, Is Transcriptionally Repressed by Methyl Jasmonic Acid in Arabidopsis. *Plant Physiol.* **145**, 863-874 (2007).
40. Wang, G. et al. A Genome-Wide Functional Investigation into the Roles of Receptor-Like Proteins in Arabidopsis. *Plant Physiol.* **147**, 503-517 (2008).
41. Widemann, E. et al. The amidohydrolases IAR3 and ILL6 contribute to jasmonoyl-isoleucine hormone turnover and generate 12-hydroxyjasmonic acid upon wounding in *Arabidopsis* leaves. *J. Biol. Chem.* **288**, 31701-31714 (2013).
42. Yang, T. et al. The SUPPRESSOR of MAX2 1 (SMAX1)-Like SMXL6, SMXL7 and SMXL8 act as negative regulators in response to drought stress in Arabidopsis. *Plant Cell Physiol.* **61**, 1477-1492 (2020).
43. Ali, M. A. et al. Transcription factors WRKY11 and WRKY17 are involved in abiotic stress responses in Arabidopsis. *J. Plant Physiol.* **226**, 12-21 (2018).
44. Renau-Morata, B. et al. CDF transcription factors: plant regulators to deal with extreme environmental conditions. *J. Exp. Bot.* **71**, 3803-3815 (2020).
45. Zhao, P. et al. ERF1 inhibits lateral root emergence by promoting local auxin accumulation and repressing *ARF7* expression. *Cell Rep.* **42**, 112565 (2023).
46. He, K. et al. Cryptic phylogeographic history sheds light on the generation of species diversity in sky-island mountains. *J. Biogeogr.* **46**, 2232-2247 (2019).
47. Capblancq, T. & Forester, B. R. Redundancy analysis: A Swiss Army Knife for landscape genomics. *Methods Ecol. Evol.* **12**, 2298-2309 (2021).
48. Gougherty, A. V., Keller, S. R. & Fitzpatrick, M. C. Maladaptation, migration and extirpation fuel climate change risk in a forest tree species. *Nat. Clim. Chang.* **11**, 166-171 (2021).
49. Robinson, J., Kyriazis, C. C., Yuan, S. C. & Lohmueller, K. E. Deleterious variation in natural populations and implications for conservation genetics. *Annu. Rev. Anim. Biosci.* **11**, 93-114 (2023).
50. Waldvogel, A.-M. et al. Evolutionary genomics can improve prediction of species' responses to climate change. *Evol. Lett.* **4**, 4-18 (2020).
51. Sandercock, A. M., Westbrook, J. W., Zhang, Q., & Holliday, J. A. A genome-guided strategy for climate resilience in American chestnut restoration populations. *Proc. Natl Acad. Sci. USA* **121**, e2403505121 (2024).
52. Nosil, P., Funk, D. J. & Ortiz-Barrientos, D. Divergent selection and heterogeneous genomic divergence. *Mol. Ecol.* **18**, 375-402 (2009).
53. Battlay, P. et al. Large haploblocks underlie rapid adaptation in the invasive weed *Ambrosia artemisiifolia*. *Nat. Commun.* **14**, 1717 (2023).
54. Sandoval-Castillo, J. et al. Adaptation of plasticity to projected maximum temperatures and across climatically defined bioregions. *Proc. Natl Acad. Sci. USA* **117**, 17112-17121 (2020).
55. Ballinger, M. A., Mack, K. L., Durkin, S. M., Riddell, E. A. & Nachman, M. W. Environmentally robust *cis*-regulatory changes underlie rapid climatic adaptation. *Proc. Natl Acad. Sci. USA* **120**, e2214614120 (2023).
56. Merilä, J. & Hendry, A. P. Climate change, adaptation, and phenotypic plasticity: the problem and the evidence. *Evol. Appl.* **7**, 1-14 (2014).

57. Feng, J. et al. Integrating evolutionary genomics of forest trees to inform future tree breeding amidst rapid climate change. *Plant Commun.* 101044 (2024).

58. Vinton, A. C., Gascoigne, S. J., Sepil, I. & Salguero-Gómez, R. Plasticity's role in adaptive evolution depends on environmental change components. *Trends Ecol. Evol.* **37**, 1067-1078 (2022).

59. Aitken, S. N. & Whitlock, M. C. Assisted gene flow to facilitate local adaptation to climate change. *Annu. Rev. Ecol. Evol. Syst.* **44**, 367-388 (2013).

60. Lotterhos, K. E. Principles in experimental design for evaluating genomic forecasts. *Methods Ecol. Evol.* **26**, 706-717 (2024).

61. Lind, B. M. et al. How useful is genomic data for predicting maladaptation to future climate? *Glob. Chang. Biol.* **30**, e17227 (2024).

METHODS

Genome sequencing and assembly

Fresh young leaves of a wild *P. lasiocarpa* individual located in Xinqiao Town, Meishan City, Sichuan Province, China (103° 51' 36"E, 30° 9' 36" N) were harvested and frozen in liquid nitrogen. High-quality genomic DNA was extracted from leaves using the CTAB procedure [61]. For the long-read sequencing, libraries with >20 Kbp DNA fragments were constructed and sequenced on PromethION platform with Oxford Nanopore Technologies (ONT). For short-read sequencing, 150 bp paired-end libraries with an insert size of 350 bp were generated and sequenced on Illumina HiSeq X Ten platform. To achieve chromosome-scale genome assembly, a Hi-C sequencing library was constructed and prepared with Dpnll restriction enzyme, followed by sequencing on the Illumina NovaSeq platform.

We performed the *de novo* assembly process in the following steps. Initially, the long sequencing reads, after self-correction, were assembled into contigs using NextDenovo (https://github.com/Nextomics/NextDenovo). To obtain a high-quality assembly, polishing was performed with both Nanopore reads for three rounds using Racon[62] and Illumina reads for four rounds using Nextpolish v1.0.5[63]. Heterozygous contigs were then removed from the resultant contig-level assembly using purge_haplotigs v1.1.1[64] with parameter settings -l 5 -m 66 -h 170. Next, Hi-C reads filtered by fastp v0.20.0[65] were aligned onto the contig-level assembly using bowtie2 v2.3.2[66]. Each pair of the uniquely mapped reads was then merged to cluster, orientate, and link the contigs into 19 pseudo-chromosomes using LACHESIS[67]. Finally, to validate the completeness and accuracy of the assembly, we calculated the Benchmarking Universal Single-Copy Orthologs (BUSCO)[21] score and estimated the Illumina short reads mapping rate using BCFTOOLS v1.11[68].

Gene prediction and functional annotation

Before gene prediction, preliminary transposable element (TE) annotation was performed by EDTA v1.9.3[69], and TEs annotated as “LTR/unknown” were re-

classified using TEsorter v1.2.5[70]. The TE libraries were then used to mask the whole genome sequences using RepeatMasker v4.10[71]. To predict the protein-coding genes, we integrated three strategies including homology-based, RNA-seq-based, and *ab initio* prediction. First, we mapped the protein sequences of six species (*Populus trichocarpa*, *Populus euphratica*, *Salix brachista*, *Salix purpurea*, *Arabidopsis thaliana* and *Vitis vinifera*) to *P. lasiocarpa* genome by TBLASTN (ncbi-BLAST v2.2.28)[72], and parsed the resultant alignments for homology-based predictions using Genewise v2.4.1[73]. Then, assembled transcripts from RNA sequencing reads of leaf and stem tissues, obtained using both genome-free and genome-guided methods with Trinity v2.8.4[74], were aligned to the reference genome using PASA v2.4.1[75] to conduct RNA-seq-based prediction. Additionally, Augustus v3.3.2[76] was used for *ab initio* gene prediction, utilizing gene models predicted through both homology-based methods and RNA-seq data. Finally, EvidenceModeler v1.1.1[77] was employed to integrate all above gene models into a comprehensive gene set, which was subsequently refined through three rounds of PASA v2.4.1.

Gene functional annotation was conducted based on BLAST with 1e-5 E-value cutoff against 9 well-known public protein databases: the protein families database (Pfam), the NCBI non-redundant protein database (NR), the interproscan database, the KEGG database, the Swiss-Prot protein database, the Eukaryotic Orthologous Groups of proteins (KOG), the Clusters of Orthologous Groups of protein (COG), the Translated European Molecular Biology Laboratory (TrEMBL) database and the Gene Ontology (GO) database. The putative domains and GO terms of genes were identified using the InterProScan v5.32-71.0[78] program with default parameters.

Genome resequencing, read mapping, and variant calling

A total of 200 *P. lasiocarpa* wild accessions were collected from 22 natural populations throughout the natural distribution of this species for whole-genome resequencing. Sampled individuals were at least 100m apart from each other within each population. Genomic DNA was extracted from fresh mature leaves using a DNeasy® Tissue Kit (QIAGEN). Illumina paired-end libraries of 150 bp in length were constructed and

829 sequenced on Illumina NovaSeq 6000 platform with a target coverage of at least 20×
830 per individual.

831 Prior to read mapping, raw sequencing reads were trimmed and filtered using Fastp
832 v0.20.0. The parameter settings of '-f 5 –F 5 -t 5 –T 5' were used to trim five bases from
833 both the front and tail of paired-end reads. The parameters '-n 0 -q 20 –u 20' were used
834 to retain reads with no N base, a Phred quality greater than 20, and less than 20%
835 unqualified bases. The quality of reads was assessed using FastQC v.0.11.7[79] before
836 and after trimming. The remaining read pairs were then mapped to our high-quality
837 reference genome with BWA-MEM[80] and sorted with SAMtools v.1.9[81] with
838 default parameters. PCR duplicates were marked using MarkDuplicates tool from
839 Picard v.2.18.21 (https://broadinstitute.github.io/picard/). For genomic variant
840 identification, SNP and Indel calling was performed using Genome Analysis Toolkit
841 (GATK v.3.8.1)[82] and its subcomponents HaplotypeCaller to obtain per-sample
842 variants. Joint genotyping was then conducted using the GenotypeGVCFs tool with the
843 option "-all-sites" to output both variant and non-variant sites. SNPs and Indels were
844 filtered using VCFtools v0.1.16 [83], retaining bi-allelic variants with a genotype
845 missing rate of less than 20%, after treating genotypes with read depth (DP) < 5 and
846 genotype quality (GQ) < 10 as missing. SVs were called with DELLY v0.8.38[26], and
847 those longer than 50 bp with precise breakpoints and a genotype missing rate of less
848 than 20% were retained, after treating genotypes with DP < 5 and GQ < 10 as missing.
849 Finally, SNPable (https://lh3lh3.users.sourceforge.net/snpable.shtml) was implemented
850 to mask genomic regions in which reads were not uniquely mapped and the variants
851 located in these regions were further filtered.

852

853 **Phylogenetic, Admixture, and Population Structure Analyses**

854 To analyze population structure, we retained only SNPs with a minor allele frequency
855 (MAF) greater than 5%. Highly correlated SNPs were excluded by performing LD-
856 based SNP pruning using PLINK v1.90b6.18[84] with the parameter setting "--indep-
857 pairwise 50 10 0.2" (any SNP with a correlation coefficient (r^2) >0.2 with another SNP
858 within the sliding windows of 50 SNPs and advancing steps of 10 SNPs across the

genome was removed). A Neighbor-joining phylogenetic tree was constructed using PLINK and MEGA-X[85], and visualized in Figtree v1.4.4 (http://tree.bio.ed.ac.uk/software/figtree/). A principal component analysis (PCA) was also conducted to further evaluate the genetic structure using smartpca program in EIGENSOFT v.7.2.1[86]. ADMIXTURE v1.3.0[87] was employed to examine population structure across all individuals, with the number of population ancestries of predefined number of genetic clusters *K* set from 1 to 10. The most suitable number of ancestries was determined by the *K* value with the lowest cross-validation error. Additionally, to evaluate and validate the quality of SVs detected, we performed population structure analysis on the pruned SVs dataset using the same method and parameters.

Genetic diversity, linkage disequilibrium (LD) and population differentiation

Intra-group nucleotide diversity (π) and inter-group genetic divergence (F_{ST} and d_{XY}) were calculated over 100 Kbp non-overlapping window after accounting for both the polymorphic and monomorphic sites using the program pixy v1.0.4.beta1 [88]. For LD decay evaluation, the squared correlation coefficient (r^2) for all pairs of SNPs with MAF > 0.05 within a 200-Kbp window was computed and plotted using PopLDdecay v3.41 [89]. To further account for the influence of the number of individuals used in the calculation, we also randomly sampled 10 individuals from each group to calculate these parameters.

Estimation of demographic history and divergence time

The ancient and more recent demographic history were estimated using pairwise sequentially Markovian coalescent model (PSMC v0.6.5-r67 [90]) and SMC++ v1.15.4 [91], separately. Assuming a mutation rate of 3.75×10^{-8} (mutations per site per generation) and complying with 15 years as the generation [92], the scaled results were then converted into years and effective population size (*Ne*). PSMC analyses were performed for each group of 10 selected individuals, with 10 bootstraps per individual, employing the parameter settings -N25 -r5 -p "4+25*2+4+6". The median estimate

across 10 individuals was used to represent the fluctuations in *Ne* for each group. To infer the more recent demographic history, VCF file with high-quality polymorphic SNPs was converted to SMC format using the vcf2smc command in SMC++ and then the *estimate* command was run on each group with default parameters. To estimate divergence times, vcf2smc and split commands in SMC ++ program were run on the VCF file for each group pair with default parameters.

To explore the pattern of gene flow in the phylogenetic context, the pruned common SNP set was used and *P. wilsonii* (belong to the section *Leucoides* same as *P. lasiocarpa*) was selected as an outgroup. Then, the migration events were inferred by TreeMix v. 1.13 [93] with the parameters '-bootstrap 5000 -m 0-5 (-m the migration event)'. The identity-by-descent (IBD) blocks among all individuals were detected using beagle v4.1[94] with the following parameters 'window = 100,000; overlap = 10,000; ibdtrim = 100; ibdlod = 5; ibdcm=1e-5'.

Identification of genomic regions under selection

To identify genomic regions with abnormal population structure that may be under selection and show heterogenous patterns of relatedness, we applied local PCA to 180 individuals from the western and eastern populations using the R package *lostruct* v0.0.0.9000 [25]. Depending on the LD decay and the need to capture meaningful selection signals, we selected a window size of 250 SNPs for this analysis. The *P. lasiocarpa* genome was first divided into 40,380 contiguous and non-overlapping windows, each containing 250 SNPs. Windows that exhibited unusually large sizes, exceeding 20 Kbp in physical length, were removed due to the likely influence of a high proportion of repetitive sequences. To measure the similarity of individual relatedness across windows, a Euclidian distance matrix was computed and visualized using a multidimensional scaling (MDS) transformation. Window with extreme MDS1 values (top 0.5% and bottom 0.5% of MDS1 values) were defined as outlier windows. We further performed PCA and constructed the Neighbor-joining phylogenetic tree for the top outlier regions, bottom outlier regions and background regions, respectively.

As the two sets of outlier windows exhibited phylogenetic clustering topologies

consistent with signatures of divergent and balancing selection, we conducted the following analyses to further assess selection by comparing them with the remaining background portions of the genome: (1) intra-group nucleotide diversity (π) and inter-group genetic divergence (F_{ST} and d_{XY}) were calculated within and between groups of western and eastern populations using the program pixy v1.0.4.beta1; (2) Tajima's D statistics were calculated using VCFtools in 10 Kbp non-overlapping windows separately for western and eastern populations; (3) a composite likelihood ratio statistic (CLR) based on the genome-wide site frequency spectrum (SFS) of polarized SNPs was computed using SweepFinder2 [95] with 2 Kbp non-overlapping windows separately for western and eastern populations; (4) a cross-population composite likelihood ratio (XP-CLR) score was calculated using XP-CLR package [96] with 1 Kbp non-overlapping windows to specifically test for the signals of divergent selection; (5) a beta statistic (β) was computed by BetaScan2 [97] with 1 Kbp non-overlapping windows based on the genome-wide SFS of polarized SNPs was used to specifically test for signatures of long-term balancing selection. Finally, the structures of candidate genes in candidate regions were exhibited by R package gggenes (https://github.com/wilkox/gggenes).

Detection of environment-associated genetic variants

To screen for locally adaptive environmental variants, we extracted and downloaded a total of 29 environmental variables corresponding to the geographical coordinates of the population collection sites (Supplementary Table 14). These variables included nineteen climate variables related to temperature and precipitation, and water vapor pressure (kPa) in the period of 1970-2000, with 30sec resolution, all retrieved from WorldClim public database (https://www.worldclim.org). Additionally, four soil variables in 2017 at a depth of 5-15 meters with a 1000-meter resolution were downloaded from the SoilGrids website (https://soilgrids.org). Ultraviolet (UV) radiation variables in the period of 2004-2013 for each month, with a 15 arc-minutes resolution, were obtained from glUV dataset (https://www.ufz.de/gluv/) and subsequently transformed to five variables, including UV radiations for each of the four

quarters and the entire year.

We retained common variants (MAF > 5%), resulting in a total of 5,315,353 SNPs, 687,429 indels and 27,980 SVs, and employed two approaches to identify environment-associated variants. First, we used latent factor mixed modeling (LFMM)[29], implemented in the R package LEA v3.2.0 [98], to search for significant associations between allele frequencies and each of the 29 environmental variables. This analysis was conducted with two latent factors, based on the optimal number of ancestry clusters inferred with ADMIXTURE acorss the 20 populations, to account for the influence of population structure. For each environmental variable, LFMM was run with 5 repetitions, including a burn-in of 5,000 cycles followed by 10,000 iterations. The median of the resulting z-scores was calculated across the five runs, recalibrated by lambda, and the resulting *P-values* were adjusted for multiple testing using the false discovery rate (FDR) method, with an FDR of 5% set as the significance threshold. Furthermore, we employed a linear mixed model approach using the program GEMMA v 0.98.3 [30] to perform genome-wide environmental association studies, treating the environment as phenotype data. This method utilized a centered kinship matrix (-gk 1) generated from all 6,030,762 variants to account for relatedness among individuals and population structure. Similar to LFMM, we applied an FDR < 5% to control for multiple testing across the variant dataset.

Finally, to assess the reliability of the identified adaptive variants, we evaluated allele frequencies turnover along the environmental gradient and compared the patterns of these changes between the identified adaptive variants and a set of neutral references with the same number of variants. Following the method used in Aguirre-Liguori et al. 2021 [4], this analysis was conducted using machine learning algorithms implemented in the R package 'gradientForest' [99] to detect non-linear change in allele frequencies (response variables) along the climate gradient (predictor). We ran gradient forest with parameters "ntree=400, maxLevel= log2(0.368*n/2), corr.threshold=0.40" and calculated the cumulative importance of allele frequency changes as the sum of the split importance along climatic variables. The allele frequencies turnover along the environmental gradient was visualized by R package ggplot2. Additionally, to further

evaluate the impact of geography and environment on shaping genomic variation of adaptive and neutral variants, we used linearized F_{ST} (F_{ST} /1- F_{ST}) to investigate isolation by distance (IBD) and isolation by environment (IBE) through Mantel and partial Mantel tests, respectively, with Euclidean distance based on all scaled environmental variables used as the measure of environmental distance.

Characterization of haploblocks

To identify genomic regions displaying abnormal population structure potentially generated by haploblocks or inversions, we conducted local PCA analysis using R package "lostruct". This analysis was conducted with 60 SNP-wide windows (averaging 4,642bp) for each chromosome, aiming to capture smaller, more precise regions that could be grouped as haploblocks in subsequent analyses. We calculated Euclidean distances between PCA maps (using the first two principal components) to assess relatedness among windows and visualized these distances using MDS scores plotted against the positions of each window on the chromosome. Three-dimensional MDS axes were utilized to improve the detection of potential inversions. We defined genomic regions with at least ten adjacent windows having a z-score >1.5 as preliminary candidate haploblocks.

To provide further evidence for MDS outliers potentially caused by haploblocks, we conducted additional analyses to verify the following genomic signatures: (1) PCA of all SNPs within the candidate region should reveal three distinct clusters corresponding to 0/0, 0/1, and 1/1 genotypes; (2) the 0/1 genotype should exhibit the highest heterozygosity compared to 0/0 and 1/1 genotypes; and (3) high linkage disequilibrium (LD) should be observed within the haploblock region due to recombination suppression.

We then compared π, inter-population F_{ST}, the ratio of zero-fold to four-fold synonymous variants, the number of climate adaptive loci and population-scaled recombination rate (calculated by the Interval program of LDhat [100] with parameter settings"-its 1000000 -bpen 5 -samp 2000") between haploblock regions and randomly sampled genomic regions of the same size. Finally, we performed GO enrichment

analysis using topGO v2.42.0 [101] to determine whether genes in haploblock regions were enriched for specific biological functions.

Stress experimental design and RNA sequencing

Mature seeds were collected from the individuals of the West (103° 7' 12" E, 28° 43' 12" N) and East (109° 28' 48" E, 29° 59' 24" N) ecotypes of *P. lasiocarpa*. The seeds were first germinated in petri dishes and then transferred to pots, where they were grown in a greenhouse for four months under a temperature regime of 25 °C (day) and 20 °C (night), with a 16-hour photoperiod and an 8-hour dark period. After this growth period, the seedlings from both ecotypes were divided into three groups: control, heat-stress and waterlogging-stress, with each group consisting of three biological replicates. The control group was maintained under standard conditions of 25 °C/20 °C (day/night). For the waterlogging stress group, plants were transferred to tanks and subjected to full waterlogging, with the water level 3-5cm above the soil surface, for 15 days at 25°C/20°C (day/night). The heat stress group was placed in an incubator set to 42 °C (day) and 35 °C (night) for three days. On the final day of treatment, leaf and root tissues were collected from consistent positions across all replicates, flash-frozen in liquid nitrogen, and stored at -80°C. Total RNA was then extracted from these tissues, and RNA-seq libraries were prepared and sequenced on the DNBSEQ-T7 platform, generating 150 bp paired-end reads.

Gene expression analyses

After filtering and trimming RNA reads using Trimmomatic v0.39 with default parameters, we mapped the clean reads to the reference genome using HISAT v2.2.1[102], and gene expression was quantified with StringTie[103]. The gene expression values were then normalized by Python script prepDE.py to generate reads count data. Based on this normalized data, we first created a correlation matrix and conducted PCA among the treatment samples and replicates. Genes with fewer than 10 reads were removed, and only the expressed gene were retained for downstream analyses.

1039 To quantify expression changes, DESeq2 [104] was used to test for differential
1040 expression between control and stress-treated individuals in each group of the two
1041 ecotypes in both leaf and root tissues. Differentially expressed genes (DEGs) were
1042 identified using cutoff threshold of FDR < 0.05 and -2<$\log_2$ Fold Change>2. To assess
1043 whether plastic changes in gene expression under stress conditions correlated with
1044 evolved expression divergence, we compared plastic expression changes in the West
1045 ecotype (considered more "ancestral" given its greater distance from future climate
1046 conditions) to evolved expression changes between the West and East ecotypes (the
1047 logic underlying this comparison is detailed in Results section).

1048 We first identified genes differentially expressed between the West and East
1049 ecotypes under control conditions. For these genes, we further compared the gene
1050 expression fold changes between control and stress-treated conditions in the West
1051 ecotype to the fold change in gene expression between the West and East ecotypes
1052 (Supplementary Fig. 16). To assess the correlation between plasticity and evolved
1053 divergence, we calculated Spearman's rank correlation coefficient (ρ) using the values
1054 of $\log_2$ Fold Change. Given that the comparison involved two ratios sharing a common
1055 denominator, we further accounted for potential statistical artifacts by employing a
1056 randomization and resampling procedure to generate a null distribution of correlation
1057 coefficients. The candidate gene set was randomized 10,000 times, and the correlations
1058 between plastic and evolved divergence in these permuted results were used to create a
1059 distribution for comparison to the observed correlation. Finally, genes were categorized
1060 as exhibiting adaptive plasticity if the direction of expression plasticity aligned with
1061 evolved divergence, and as maladaptive if it was opposite. We then performed Gene
1062 Ontology (GO) enrichment analysis for the adaptive plastic genes.

1063

1064 **Adaptive index**

1065 To investigate the adaptive genetic landscape of *P. lasiocarpa,* we performed a
1066 redundancy analysis (RDA) using the R package "vegan v2.6-4" [105] with the setting
1067 of K=2 to calculate the adaptive index . Only LD-pruned adaptive variants and seven
1068 uncorrelated (pairwise correlation coefficients |r| < 0.7) environment variables (i.e.

1069 BIO1, BIO4, BIO7, BIO8, BIO10, BIO15 and BIO18) were utilized. The adaptive
1070 index was then projected across the species' range to visualize geographic patterns of
1071 adaptation by R package ggplot2.
1072
1073 **Genomic offset assessment**
1074 For each sampling location, future BIOCLIM data for 19 climate variables at a 2.5
1075 arcmin resolution for the periods 2061-2080 and 2081-2100, under two shared
1076 socioeconomic pathways (SSP245 and SSP585), were downloaded from the
1077 WorldClim CMIP6 website. Data from three climate models (CMCC-ESM2, GISS-E2-
1078 1-G and MPI-ESM1-2-HR) were integrated. A machine learning approach, Gradient
1079 Forest, was used to predict the genomic offset in response to environmental shifts. The
1080 GF model was built with parameters ntrees=500, maxLevel=log2(0.368*n/2), and
1081 corr.threshold=0.5, based on 19,955 adaptive variants and 15 environment variables
1082 that had identified adaptive variants.
1083 Three metrics of potential maladaptation were calculated: local offset (population
1084 vulnerability *in situ* to new climate conditions), reverse offset (potential maladaptation
1085 if individuals could be relocated anywhere within the species range), and forward offset
1086 (minimum maladaptation assuming individuals could be moved anywhere within
1087 Eurasian continent) [47]. These metrics were visualized as the red, blue and green blue
1088 bands of an RGB image, respectively. Additionally, we assessed the variation in
1089 forward offset across different maximum allowable migration distances, including 100
1090 km, 250 km, 500 km, 1000 km, and unlimited across the Eurasian continent. The results
1091 suggested that forward offset decreased substantially with increasing migration
1092 distances, stabilizing at 500 km and beyond (Supplementary Fig. 20). Therefore,
1093 forward offset results with unlimited dispersal distance were presented and projected
1094 on the map.
1095
1096 **Assessment of genetic load**
1097 To assess the deleterious genetic load in the *P. lasiocarpa* population, variants were
1098 annotated as either synonymous or non-synonymous, and SIFT score were calculated

1099 for the non-synonymous variants using SIFT 4G annotator [106]. Variants were then
1100 classified into four categories: loss of function (LOF), deleterious (SIFT score <0.05),
1101 tolerated (SIFT score >0.05), or synonymous. Additionally, the derived versus ancestral
1102 allelic state at each SNP position was determined using est-sfs [107], with *P.*
1103 *trichocarpa* as the outgroup. The ratio of the number of derived mutations (LOF and
1104 deleterious) to the number of synonymous variants served as used as a proxy for genetic
1105 load.

References

1. Urban, M. C. et al. Improving the forecast for biodiversity under climate change. *Science* **353**, aad8466 (2016).
2. Bernatchez, L., Ferchaud, A.-L., Berger, C. S., Venney, C. J. & Xuereb, A. Genomics for monitoring and understanding species responses to global climate change. *Nat. Rev. Genet.* **25**, 165-183 (2024).
3. Martin, R. A., da Silva, C. R., Moore, M. P. & Diamond, S. E. When will a changing climate outpace adaptive evolution? *WIRES Clim. Chang.* **14**, e852 (2023).
4. Aguirre-Liguori, J. A., Ramírez-Barahona, S. & Gaut, B. S. The evolutionary genomics of species' responses to climate change. *Nat. Ecol. Evol.* **5**, 1350-1360 (2021).
5. Olson-Manning, C. F., Wagner, M. R. & Mitchell-Olds, T. Adaptive evolution: evaluating empirical support for theoretical predictions. *Nat. Rev. Genet.* **13**, 867-877 (2012).
6. Joron, M. et al. Chromosomal rearrangements maintain a polymorphic supergene controlling butterfly mimicry. *Nature* **477**, 203-206 (2011).
7. Lowry, D. B. & Willis, J. H. A widespread chromosomal inversion polymorphism contributes to a major life-history transition, local adaptation, and reproductive isolation. *PLoS Biol.* **8**, e1000500 (2010).
8. Todesco, M. et al. Massive haplotypes underlie ecotypic differentiation in sunflowers. *Nature* **584**, 602-607 (2020).
9. Harringmeyer, O. S. & Hoekstra, H. E. Chromosomal inversion polymorphisms shape the genomic landscape of deer mice. *Nat. Ecol. Evol.* **6**, 1965-1979 (2022).
10. Swaegers, J. & Koch, E. L. Gene expression studies of plastic and evolutionary responses to global warming. *Curr. Opin. Insect Sci.* **51**, 100918 (2022).
11. Campbell-Staton, S. C., Velotta, J. P. & Winchell, K. M. Selection on adaptive and maladaptive gene expression plasticity during thermal adaptation to urban heat islands. *Nat. Commun.* **12**, 6195 (2021).
12. Josephs, E. B., Van Etten, M. L., Harkess, A., Platts, A. & Baucom, R. S. Adaptive and maladaptive expression plasticity underlying herbicide resistance in an agricultural weed. *Evol. Lett.* **5**, 432-440 (2021).
13. Ghalambor, C. K. et al. Non-adaptive plasticity potentiates rapid adaptive evolution of gene expression in nature. *Nature* **525**, 372-375 (2015).
14. Isabel, N., Holliday, J. A. & Aitken, S. N. Forest genomics: Advancing climate adaptation, forest health, productivity, and conservation. *Evol. Appl.* **13**, 3-10 (2020).
15. Holliday, J. A. et al. Advances in ecological genomics in forest trees and applications to genetic resources conservation and breeding. *Mol. Ecol.* **26**, 706–717 (2017).
16. Browne, L., Wright, J. W., Fitz-Gibbon, S., Gugger, P. F., & Sork, V. L. Adaptational lag to temperature in valley oak (*Quercus lobata*) can be mitigated by genome-informed assisted gene flow. *Proc. Natl Acad. Sci. USA* **116**: 25179-25185 (2019).
17. Myers, N., Mittermeier, R. A., Mittermeier, C. G., Da Fonseca, G. A. & Kent, J. Biodiversity hotspots for conservation priorities. *Nature* **403**, 853-858 (2000).
18. Chen, Y. et al. The combination of genomic offset and niche modelling provides insights into climate change-driven vulnerability. *Nat. Commun.* **13**, 4821 (2022).
19. Davis, M. B. & Shaw, R. G. Range shifts and adaptive responses to Quaternary climate change.

Science **292**, 673-679 (2001).

20. Davis, M. B., Shaw, R. G. & Etterson, J. R. Evolutionary responses to changing climate. *Ecology* **86**, 1704-1714 (2005).

21. Simão, F. A., Waterhouse, R. M., Ioannidis, P., Kriventseva, E. V. & Zdobnov, E. M. BUSCO: assessing genome assembly and annotation completeness with single-copy orthologs. *Bioinformatics* **31**, 3210-3212 (2015).

22. Charlesworth, D. Balancing selection and its effects on sequences in nearby genome regions. *PLoS Genet.* **2**, e64 (2006).

23. Han, F. et al. Gene flow, ancient polymorphism, and ecological adaptation shape the genomic landscape of divergence among Darwin's finches. *Genome Res.* **27**, 1004-1015 (2017).

24. Guerrero, R. F. & Hahn, M. W. Speciation as a sieve for ancestral polymorphism. *Mol. Ecol.* **26**, 5362-5368 (2017).

25. Li, H. & Ralph, P. Local PCA Shows How the Effect of Population Structure Differs Along the Genome. *Genetics* **211**, 289-304 (2019).

26. Bhattarai, K. K., Atamian, H. S., Kaloshian, I. & Eulgem, T. WRKY72-type transcription factors contribute to basal immunity in tomato and Arabidopsis as well as gene-for-gene resistance mediated by the tomato *R* gene *Mi-1*. *Plant J.* **63**, 229-240 (2010).

27. Nomoto, Y., Kubozono, S., Yamashino, T., Nakamichi, N. & Mizuno, T. Circadian Clock- and PIF4-Controlled Plant Growth: A Coincidence Mechanism Directly Integrates a Hormone Signaling Network into the Photoperiodic Control of Plant Architectures in *Arabidopsis thaliana*. *Plant Cell Physiol.* **53**, 1950-1964 (2012).

28. Ding, Z., Millar, A. J., Davis, A. M. & Davis, S. J. TIME FOR COFFEE Encodes a Nuclear Regulator in the *Arabidopsis thaliana* Circadian Clock. *Plant Cell* **19**, 1522-1536 (2007).

29. Frichot, E., Schoville, S. D., Bouchard, G. & François, O. Testing for associations between loci and environmental gradients using latent factor mixed models. *Mol. Bio. Evol.* **30**, 1687-1699 (2013).

30. Zhou, X. & Stephens, M. Genome-wide efficient mixed-model analysis for association studies. *Nat. Genet.* **44**, 821-824 (2012).

31. Vanholme, R., Demedts, B., Morreel, K., Ralph, J. & Boerjan, W. Lignin Biosynthesis and Structure. *Plant Physiol.* **153**, 895-905 (2010).

32. Pascual, M. B. et al. Biosynthesis and Metabolic Fate of Phenylalanine in Conifers. *Front Plant Sci.* **7**, 1030 (2016).

33. Wellenreuther, M. & Bernatchez, L. Eco-Evolutionary Genomics of Chromosomal Inversions. *Trends Ecol. Evol.* **33**, 427-440 (2018).

34. Savolainen, O., Lascoux, M. & Merilä, J. Ecological genomics of local adaptation. *Nat. Rev. Genet.* **14**, 807-820 (2013).

35. Kirkpatrick, M. & Barton, N. Chromosome Inversions, Local Adaptation and Speciation. *Genetics* **173**, 419-434 (2006).

36. McVean, G. A. & Charlesworth, B. The effects of Hill-Robertson interference between weakly selected mutations on patterns of molecular evolution and variation. *Genetics* **155**, 929-944 (2000).

37. Schaal, S. M., Haller, B. C. & Lotterhos, K. E. Inversion invasions: when the genetic basis of local adaptation is concentrated within inversions in the face of gene flow. *Philos. Trans. R. Soc. Lond. B. Bio. Sci.* **377**, 20210200 (2022).

38. Liu, C. & Mehdy, M. C. A Nonclassical Arabinogalactan Protein Gene Highly Expressed in Vascular Tissues, *AGP31*, Is Transcriptionally Repressed by Methyl Jasmonic Acid in Arabidopsis. *Plant Physiol.* **145**, 863-874 (2007).
39. Wang, G. et al. A Genome-Wide Functional Investigation into the Roles of Receptor-Like Proteins in Arabidopsis. *Plant Physiol.* **147**, 503-517 (2008).
40. Widemann, E. et al. The amidohydrolases IAR3 and ILL6 contribute to jasmonoyl-isoleucine hormone turnover and generate 12-hydroxyjasmonic acid upon wounding in *Arabidopsis* leaves. *J. Biol. Chem.* **288**, 31701-31714 (2013).
41. Yang, T. et al. The SUPPRESSOR of MAX2 1 (SMAX1)-Like SMXL6, SMXL7 and SMXL8 act as negative regulators in response to drought stress in Arabidopsis. *Plant Cell Physiol.* **61**, 1477-1492 (2020).
42. Ali, M. A. et al. Transcription factors WRKY11 and WRKY17 are involved in abiotic stress responses in Arabidopsis. *J. Plant Physiol.* **226**, 12-21 (2018).
43. Renau-Morata, B. et al. CDF transcription factors: plant regulators to deal with extreme environmental conditions. *J. Exp. Bot.* **71**, 3803-3815 (2020).
44. Zhao, P. et al. ERF1 inhibits lateral root emergence by promoting local auxin accumulation and repressing *ARF7* expression. *Cell Rep.* **42**, 112565 (2023).
45. He, K. et al. Cryptic phylogeographic history sheds light on the generation of species diversity in sky-island mountains. *J. Biogeogr.* **46**, 2232-2247 (2019).
46. Capblancq, T. & Forester, B. R. Redundancy analysis: A Swiss Army Knife for landscape genomics. *Methods Ecol. Evol.* **12**, 2298-2309 (2021).
47. Gougherty, A. V., Keller, S. R. & Fitzpatrick, M. C. Maladaptation, migration and extirpation fuel climate change risk in a forest tree species. *Nat. Clim. Chang.* **11**, 166-171 (2021).
48. Robinson, J., Kyriazis, C. C., Yuan, S. C. & Lohmueller, K. E. Deleterious variation in natural populations and implications for conservation genetics. *Annu. Rev. Anim. Biosci.* **11**, 93-114 (2023).
49. Waldvogel, A.-M. et al. Evolutionary genomics can improve prediction of species' responses to climate change. *Evol. Lett.* **4**, 4-18 (2020).
50. Sandercock, A. M., Westbrook, J. W., Zhang, Q., & Holliday, J. A. A genome-guided strategy for climate resilience in American chestnut restoration populations. *Proc. Natl Acad. Sci. USA* **121**, e2403505121 (2024).
51. Nosil, P., Funk, D. J. & Ortiz-Barrientos, D. Divergent selection and heterogeneous genomic divergence. *Mol. Ecol.* **18**, 375-402 (2009).
52. Battlay, P. et al. Large haploblocks underlie rapid adaptation in the invasive weed *Ambrosia artemisiifolia*. *Nat. Commun.* **14**, 1717 (2023).
53. Sandoval-Castillo, J. et al. Adaptation of plasticity to projected maximum temperatures and across climatically defined bioregions. *Proc. Natl Acad. Sci. USA* **117**, 17112-17121 (2020).
54. Ballinger, M. A., Mack, K. L., Durkin, S. M., Riddell, E. A. & Nachman, M. W. Environmentally robust *cis*-regulatory changes underlie rapid climatic adaptation. *Proc. Natl Acad. Sci. USA* **120**, e2214614120 (2023).
55. Merilä, J. & Hendry, A. P. Climate change, adaptation, and phenotypic plasticity: the problem and the evidence. *Evol. Appl.* **7**, 1-14 (2014).
56. Feng, J. et al. Integrating evolutionary genomics of forest trees to inform future tree breeding amidst rapid climate change. *Plant Commun.* 101044 (2024).

1237 57. Vinton, A. C., Gascoigne, S. J., Sepil, I. & Salguero-Gómez, R. Plasticity's role in adaptive
1238 evolution depends on environmental change components. *Trends Ecol. Evol.* **37**, 1067-1078
1239 (2022).
1240 58. Aitken, S. N. & Whitlock, M. C. Assisted gene flow to facilitate local adaptation to climate
1241 change. *Annu. Rev. Ecol. Evol. Syst.* **44**, 367-388 (2013).
1242 59. Lotterhos, K. E. Principles in experimental design for evaluating genomic forecasts. *Methods*
1243 *Ecol. Evol.* **26**, 706-717 (2024).
1244 60. Lind, B. M. et al. How useful is genomic data for predicting maladaptation to future climate?
1245 *Glob. Chang. Biol.* **30**, e17227 (2024).
1246 61. Rogers, S. O. & Bendich, A. J. Extraction of DNA from milligram amounts of fresh, herbarium
1247 and mummified plant tissues. *Plant Mol. Biol.* **5**, 69-76 (1985).
1248 62. Vaser, R., Sović, I., Nagarajan, N. & Šikić, M. Fast and accurate de novo genome assembly
1249 from long uncorrected reads. *Genome Res.* **27**, 737-746 (2017).
1250 63. Hu, J., Fan, J., Sun, Z. & Liu, S. NextPolish: a fast and efficient genome polishing tool for long-
1251 read assembly. *Bioinformatics* **36**, 2253-2255 (2020).
1252 64. Roach, M. J., Schmidt, S. A. & Borneman, A. R. Purge Haplotigs: allelic contig reassignment
1253 for third-gen diploid genome assemblies. *BMC Bioinformatics* **19**, 460 (2018).
1254 65. Chen, S., Zhou, Y., Chen, Y. & Gu, J. fastp: an ultra-fast all-in-one FASTQ preprocessor.
1255 *Bioinformatics* **34**, i884-i890 (2018).
1256 66. Langmead, B. & Salzberg, S. L. Fast gapped-read alignment with Bowtie 2. *Nat. Methods* **9**,
1257 357-359 (2012).
1258 67. Burton, J. N. et al. Chromosome-scale scaffolding of de novo genome assemblies based on
1259 chromatin interactions. *Nat. Biotechnol.* **31**, 1119-1125 (2013).
1260 68. Li, H. A statistical framework for SNP calling, mutation discovery, association mapping and
1261 population genetical parameter estimation from sequencing data. *Bioinformatics (Oxford,*
1262 *England)* **27**, 2987-2993 (2011).
1263 69. Ou, S. et al. Benchmarking transposable element annotation methods for creation of a
1264 streamlined, comprehensive pipeline. *Genome Biol.* **20**, 275 (2019).
1265 70. Zhang, R.-G. et al. TEsorter: an accurate and fast method to classify LTR-retrotransposons in
1266 plant genomes. *Hortic. Res.* **9**, uhac017 (2022).
1267 71. Tempel, S. Using and understanding RepeatMasker. *Methods Mol. Biol.* **859**, 29-51 (2012).
1268 72. Camacho, C. et al. BLAST+: architecture and applications. *BMC bioinformatics* **10**, 1-9 (2009).
1269 73. Birney, E., Clamp, M. & Durbin, R. GeneWise and genomewise. *Genome Res.* **14**, 988-995
1270 (2004).
1271 74. Haas, B. J. et al. De novo transcript sequence reconstruction from RNA-seq using the Trinity
1272 platform for reference generation and analysis. *Nat. protoc.* **8**, 1494-1512 (2013).
1273 75. Haas, B. J. et al. Automated eukaryotic gene structure annotation using EVidenceModeler and
1274 the Program to Assemble Spliced Alignments. *Genome biol.* **9**, 1-22 (2008).
1275 76. Stanke, M. & Morgenstern, B. AUGUSTUS: a web server for gene prediction in eukaryotes that
1276 allows user-defined constraints. *Nucleic Acids Res.* **33**, W465-W467 (2005).
1277 77. Haas, B. J. et al. Automated eukaryotic gene structure annotation using EVidenceModeler and
1278 the Program to Assemble Spliced Alignments. *Genome Biol.* **9**, 1-22 (2008).
1279 78. Jones, P. et al. InterProScan 5: genome-scale protein function classification. *Bioinformatics* **30**,
1280 1236-1240 (2014).

79. Davis, M. P., van Dongen, S., Abreu-Goodger, C., Bartonicek, N. & Enright, A. J. Kraken: a set of tools for quality control and analysis of high-throughput sequence data. *Methods* **63**, 41-49 (2013).
80. Li, H. Aligning sequence reads, clone sequences and assembly contigs with BWA-MEM. *arXiv preprint arXiv:1303.3997* (2013).
81. Li, H. et al. The sequence alignment/map format and SAMtools. *Bioinformatics* **25**, 2078-2079 (2009).
82. DePristo, M. A. et al. A framework for variation discovery and genotyping using next-generation DNA sequencing data. *Nat. Genet.* **43**, 491-498 (2011).
83. Danecek, P. et al. The variant call format and VCFtools. *Bioinformatics* **27**, 2156-2158 (2011).
84. Purcell, S. et al. PLINK: a tool set for whole-genome association and population-based linkage analyses. *Am. J. Hum. Genet.* **81**, 559-575 (2007).
85. Kumar, S., Stecher, G., Li, M., Knyaz, C. & Tamura, K. MEGA X: Molecular Evolutionary Genetics Analysis across Computing Platforms. *Mol. Biol. Evol.* **35**, 1547-1549 (2018).
86. Patterson, N., Price, A. L. & Reich, D. Population structure and eigenanalysis. *PLoS Genet.* **2**, e190 (2006).
87. Alexander, D. H., Novembre, J. & Lange, K. Fast model-based estimation of ancestry in unrelated individuals. *Genome Res.* **19**, 1655-1664 (2009).
88. Korunes, K. L. & Samuk, K. pixy: Unbiased estimation of nucleotide diversity and divergence in the presence of missing data. *Mol. Ecol. Resour.* **21**, 1359-1368 (2021).
89. Zhang, C., Dong, S.-S., Xu, J.-Y., He, W.-M. & Yang, T.-L. PopLDdecay: a fast and effective tool for linkage disequilibrium decay analysis based on variant call format files. *Bioinformatics* **35**, 1786-1788 (2019).
90. Liu, S. & Hansen, M. M. PSMC (pairwise sequentially Markovian coalescent) analysis of RAD (restriction site associated DNA) sequencing data. *Mol. Ecol. Resour.* **17**, 631-641 (2017).
91. Terhorst, J., Kamm, J. A. & Song, Y. S. Robust and scalable inference of population history from hundreds of unphased whole genomes. *Nat. Genet.* **49**, 303-309 (2017).
92. Ingvarsson, P. K. Multilocus patterns of nucleotide polymorphism and the demographic history of *Populus tremula*. *Genetics* **180**, 329-340 (2008).
93. Pickrell, J. & Pritchard, J. Inference of population splits and mixtures from genome-wide allele frequency data. *PLoS Genet.* **8**, e1002967 (2012).
94. Browning, B. L. & Browning, S. R. Improving the Accuracy and Efficiency of Identity-by-Descent Detection in Population Data. *Genetics* **194**, 459-471 (2013).
95. DeGiorgio, M., Huber, C. D., Hubisz, M. J., Hellmann, I. & Nielsen, R. SweepFinder2: increased sensitivity, robustness and flexibility. *Bioinformatics* **32**, 1895-1897 (2016).
96. Chen, H., Patterson, N. & Reich, D. Population differentiation as a test for selective sweeps. *Genome Res.* **20**, 393-402 (2010).
97. Siewert, K. M. & Voight, B. F. Detecting Long-Term Balancing Selection Using Allele Frequency Correlation. *Mol. Biol. Evol.* **34**, 2996-3005 (2017).
98. Frichot, E. & François, O. LEA: An R package for landscape and ecological association studies. *Methods Ecol. Evol.* **6**, 925-929 (2015).
99. Ellis, N., Smith, S. J. & Pitcher, C. R. Gradient forests: calculating importance gradients on physical predictors. *Ecology* **93**, 156-168 (2012).
100. McVean, G. & Auton, A. LDhat 2.1: a package for the population genetic analysis of

recombination. *Department of Statistics, Oxford, OX1 3TG, UK* (2007).

101. Alexa, A. & Rahnenführer, J. Gene set enrichment analysis with topGO. *Bioconductor Improv* **27**, 1-26 (2009).

102. Kim, D., Langmead, B. & Salzberg, S. L. HISAT: a fast spliced aligner with low memory requirements. *Nat. Methods* **12**, 357-360 (2015).

103. Pertea, M. et al. StringTie enables improved reconstruction of a transcriptome from RNA-seq reads. *Nat. Biotechnol.* **33**, 290-295 (2015).

104. Love, M. I., Huber, W. & Anders, S. Moderated estimation of fold change and dispersion for RNA-seq data with DESeq2. *Genome Biol.* **15**, 550 (2014).

105. Dixon, P. VEGAN, a package of R functions for community ecology. *J. Veg. Sci.* **14**, 927-930 (2003).

106. Vaser, R., Adusumalli, S., Leng, S. N., Sikic, M. & Ng, P. C. SIFT missense predictions for genomes. *Nat. Protoc.* **11**, 1-9 (2016).

107. Keightley, P. D. & Jackson, B. C. Inferring the probability of the derived vs. the ancestral allelic state at a polymorphic site. *Genetics* **209**, 897-906 (2018).

Figures

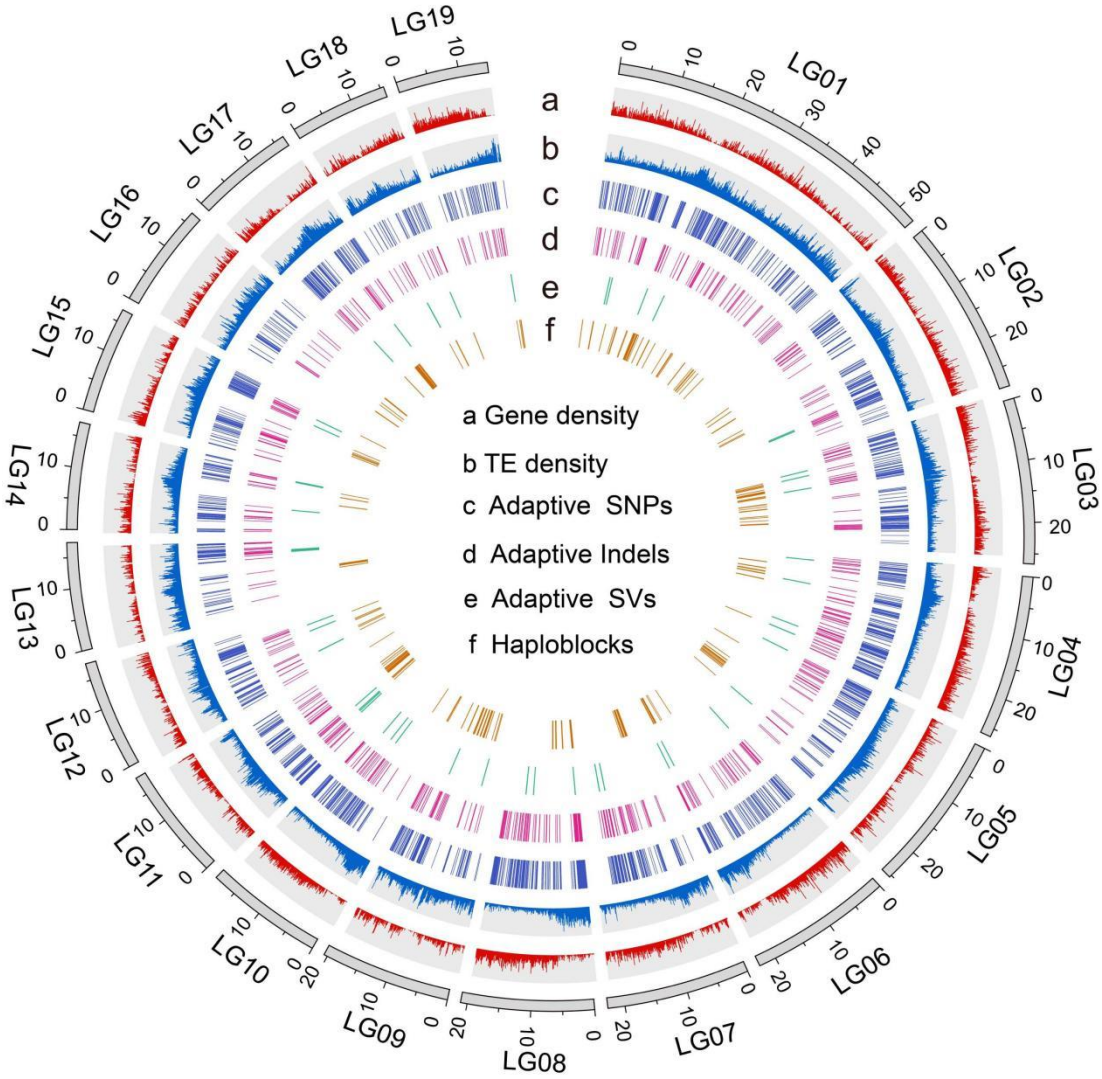

Fig. 1. Genomic features of *P. lasiocarpa* reference genome. The Circos plot displays gene density (**a**), transposable element (TE) density (**b**), distribution of putatively climatic-adaptive SNPs (**c**), INDELs (**d**), SVs (**e**), and the distribution of haploblocks (**f**).

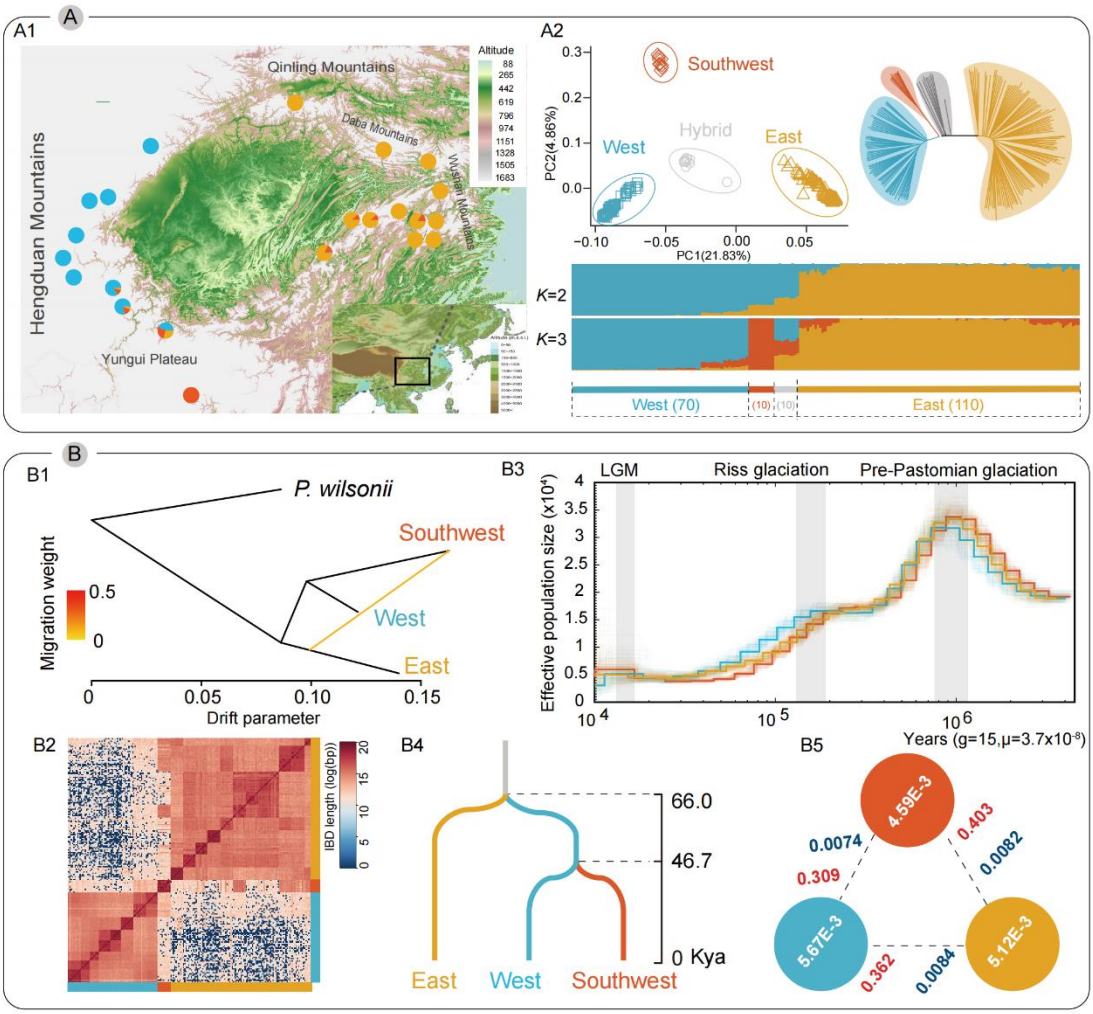

Fig. 2. Population genomic analyses of *P. lasiocarpa*. (A1) Geographic distribution of sampled *P. lasiocarpa* populations, with colors representing ancestral components inferred by ADMIXTURE at K=3. **(A2)** Neighbor-joining (NJ) phylogenetic tree, PCA, and genetic cluster plots for a K=2 and K=3, where the height of each colored segment represents the proportion of the individual's genome derived from inferred ancestral lineages. The number of individuals in each group is shown within the dashed-line box. **(B1)** Population splits and migrations among three groups of *P. lasiocarpa* using TreeMix analysis. **(B2)** Estimated haplotype sharing among individuals of *P. lasiocarpa*. The heatmap color reflects the total length of identity-by-descent (IBD) among individuals. **(B3)** Demographic history revealed by the PSMC method. For each lineage, the median estimate for all 10 selected individuals is shown with a bold line, while 100 bootstrap replicates (ten replicates for each of the 10 samples) are shown with faint lines. The gray vertical bars indicate the periods of the Last Glacial Maximum, Riss Glaciation, and Pre-Pastonian Glaciation. **(B4)** Divergence times of three groups, with timelines of splits inferred by SMC++. **(B5)** Estimation of nucleotide diversity (π), relative genetic divergence (F_{ST}), and absolute genetic divergence (d_{XY}) within and between the three lineages (red: Southwest; blue: West; orange: East).

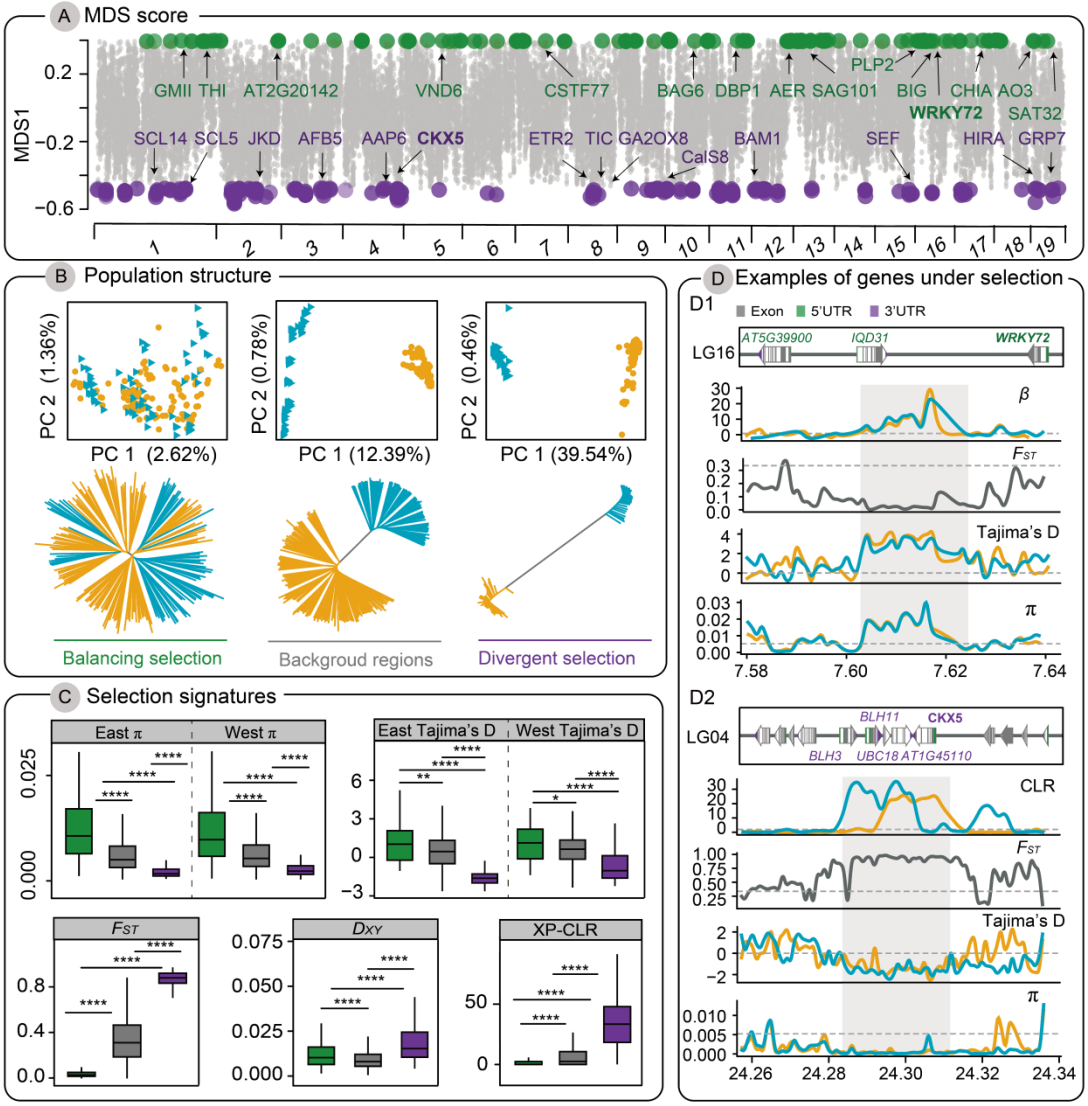

Fig. 3. Identification of balancing and divergent selection regions. (A) Characterization of MDS (multidimensional scaling) outlier regions across the genome using local PCA. Each dot represents a window containing 250 SNPs. Candidate regions under balancing selection are colored green, while those under divergent selection are colored purple. **(B)** PCA and NJ tree analyses based on SNPs from balancing selection regions, background regions, and divergent selection regions. **(C)** Comparison of π, Tajima's D, F_{ST}, d_{XY}, and XP-CLR among balancing selection regions (green), background regions (grey), and divergent selection regions (purple). Significance was determined using the Wilcoxon test (two-tailed), with asterisks indicating significance levels above the boxplot (***P<0.001, **P<0.01, *P<0.05, ns: P>0.05). **(D)** Distribution of β, CLR, F_{ST}, Tajima's D, and π around examples of candidate genes in balancing (D1) and divergent (D2) selection regions. Grey dashed lines represent the genome-wide significance level of the top 0.5% for each parameter. The structure of each candidate gene is shown in the upper box.

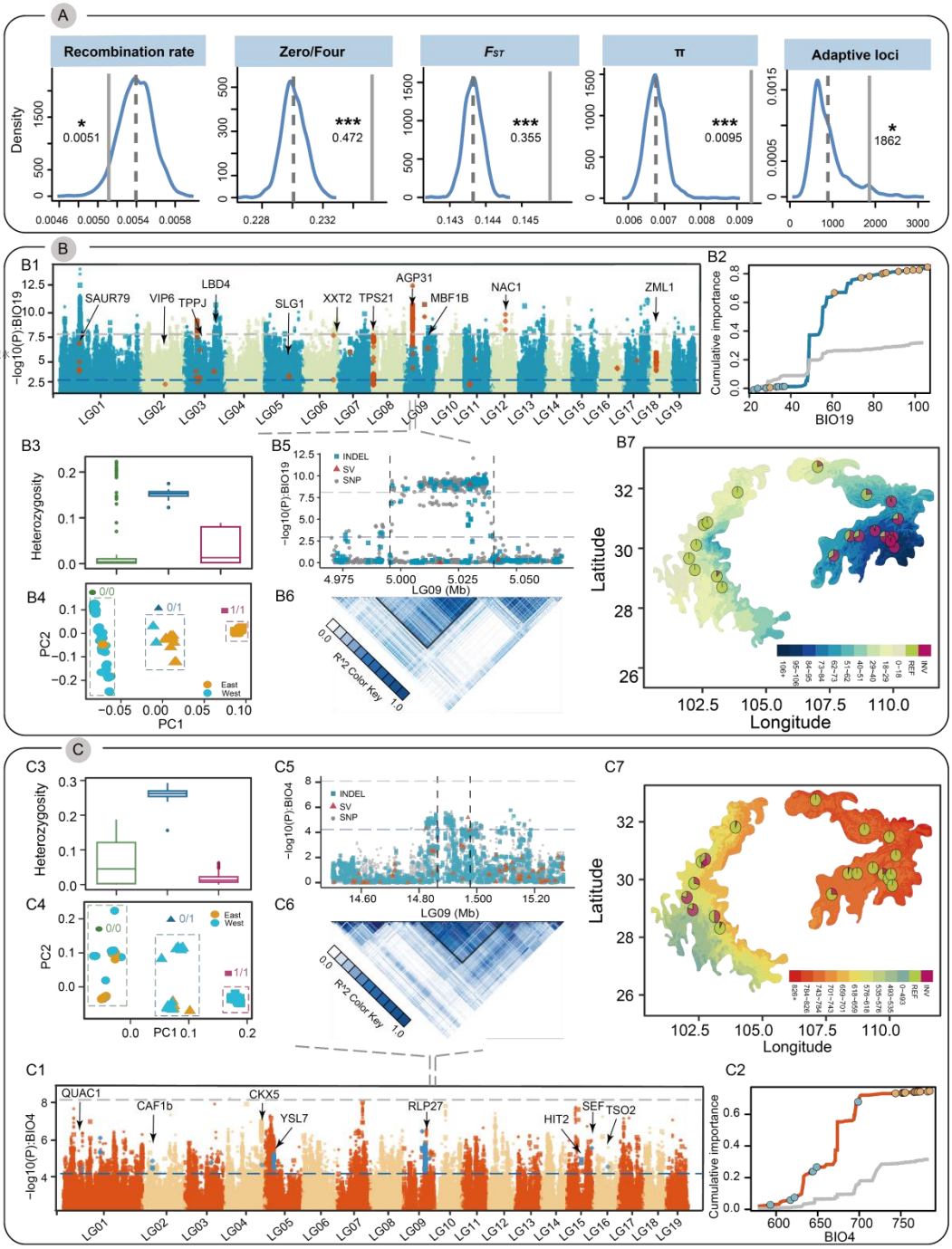

Fig. 4. Haploblocks facilitate local adaptation. (A) Assessment of genomic features of candidate haploblocks. The diagram compares recombination rate, mutation load (ratio of 0-fold to 4-fold polymorphic sites), F_{ST}, nucleotide diversity (π), and the number of adaptive loci between haploblocks (grey solid line) and permutation results from 1,000 randomizations (blue solid line). The dashed line represents the mean value across randomizations. Significance is assessed by permutation test and indicated by asterisks (*** P<0.001, ** P<0.01, * P<0.05, ns: P>0.05). **(B, C)** Two examples of haploblocks contributing to environmental adaptation: **(B1, C1)** Manhattan plots for variants associated with Precipitation of Coldest Quarter (BIO19) and Temperature Seasonality (BIO4). Red and blue circles represent adaptive variants within

haploblocks. Selected candidate genes are labeled at their respective genomic positions. Dashed horizontal lines denote significance thresholds (blue: FDR correction 0.05; grey: Bonferroni correction, adjusted P=0.05). **(B2, C2)** Cumulative importance of allelic change along environmental gradients for neutral variants (grey line) and adaptive variants associated with BIO19 (blue line) and BIO4 (orange line). **(B3, C3)** Comparison of heterozygosity within the example haploblock among clusters assigned by PCA results. **(B4, C4)** Clustering of individuals using *k*-means based on PCA results for each haploblock. **(B5, C5)** Local magnification of the Manhattan plots around the selected haploblocks. **(B6, C6)** Linkage disequilibrium (LD) block for the example haploblock, shown as mean r^2 for paired windows. **(B7, C7)** Allele frequencies of the example haploblock across 20 populations. Pie charts represent the genotype of the example haploblock based on clustering results from B4 and C4. Colors on the map represent environmental gradients across the distribution range.

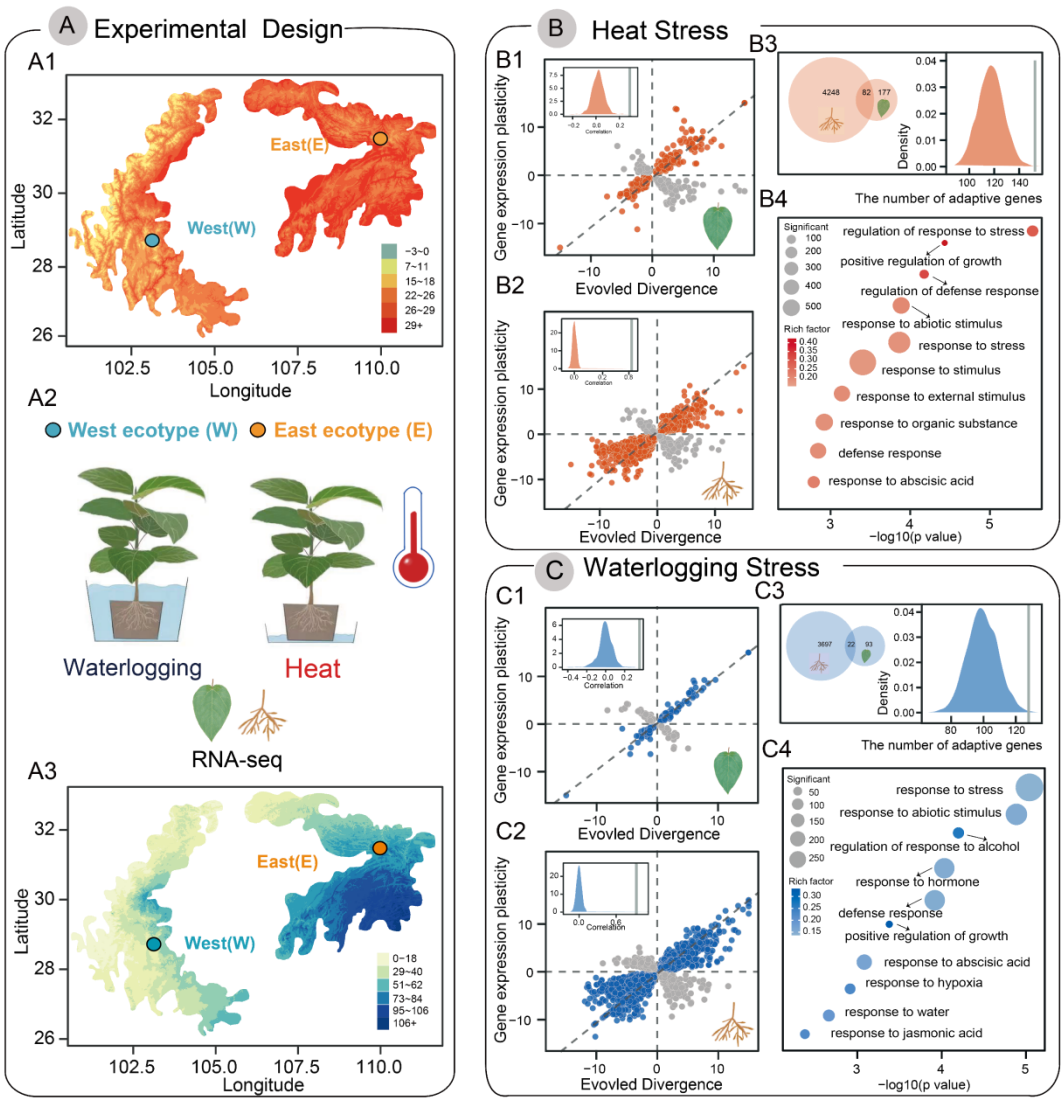

Fig. 5. Plastic and evolved changes in gene expression. (A) Experimental Design: **(A1, A3)** Environmental gradients for Maximum Temperature of the Warmest Month (top) and Precipitation of the Coldest Quarter (bottom) across the distribution range of *P. lasiocarpa*. Circles on the map indicate the locations of the experimental individuals; **(A2)** Conceptual illustration of heat and waterlogging treatments, along with RNA-seq sampling of tissues. **(B, C)** Analysis of gene expression plasticity and evolved divergence under heat and waterlogging treatments: **(B1, C1; B2, C2)** Relationship between gene expression plasticity and evolved expression divergence for leaf (top) and root (bottom) tissues. Points represent differentially expressed genes (DEGs) showing both expression plasticity and evolved expression divergence. Orange and blue points indicate genes with a positive correlation between plasticity and evolved divergence (adaptive plasticity), while grey points denote a negative association (maladaptive plasticity). Insets show that the observed correlation coefficient (grey solid lines) is more positive than the permutation results; **(B3, C3)** Venn diagrams showing the overlap of adaptive plastic genes detected in leaf and root tissues under heat and waterlogging treatments, respectively. The figure on the right displays the number of genes with signatures of environmental adaptation, as

1423 evidenced by the GEA method, in the sets of adaptive plastic genes (grey solid line)
1424 compared to the permutation results; **(B4, C4)** Representative Gene Ontology (GO)
1425 enrichment categories of adaptive plastic genes in response to heat and waterlogging
1426 stresses.

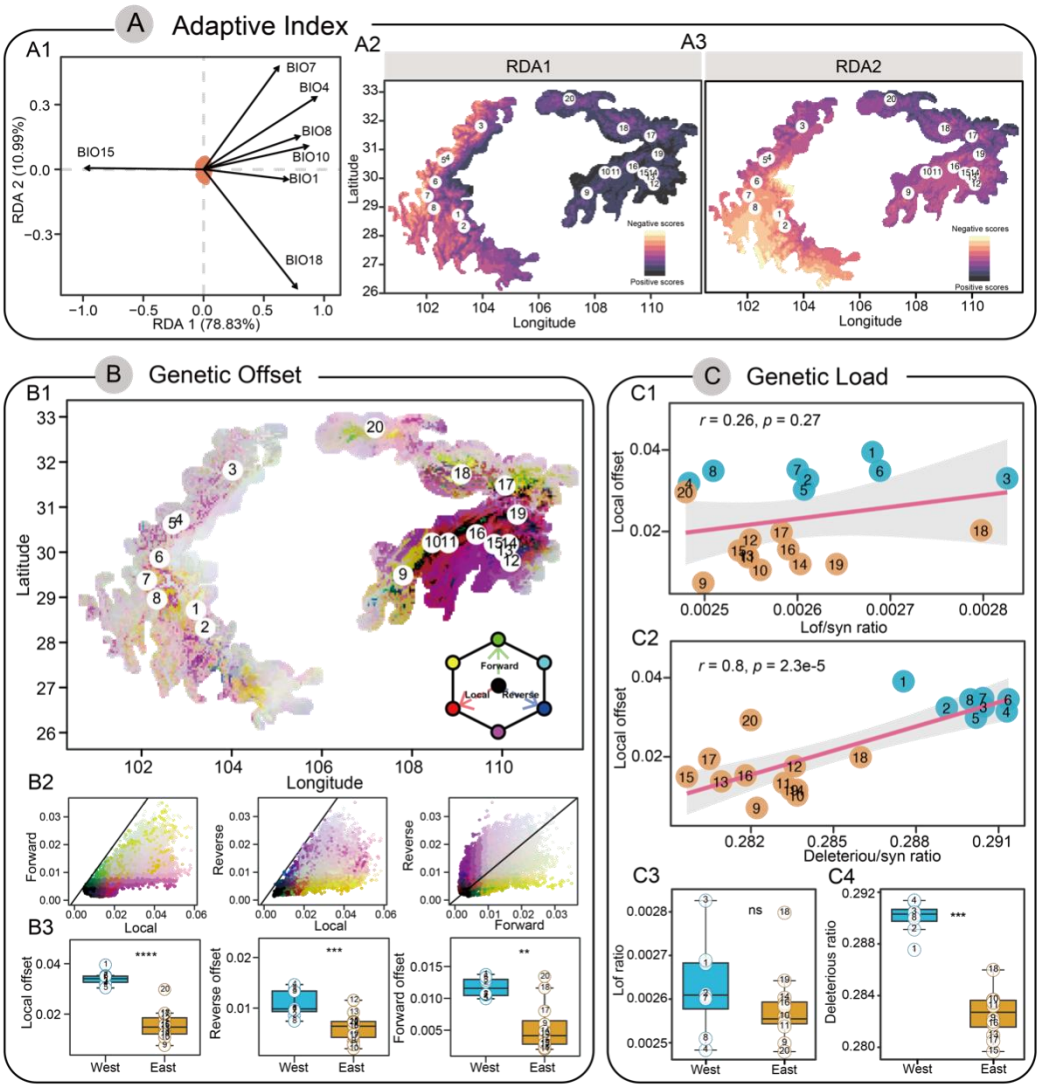

Fig. 6. Genomic vulnerability prediction in response to future climate change. (A) Adaptive landscape across species range: **(A1)** RDA results showing the association between adaptive loci and the seven climatic variables. **(A2, A3)** Spatial projection of the adaptive index along RDA1 and RDA2 across the range of *P. lasiocarpa*. **(B)** Predicted genetic offsets to future climate change under SSP245 in 2061-2080: **(B1)** RGB map depicting local (red), forward (green) and reverse (blue) offsets. Circles represent the sampled populations. **(B2)** Bivariate scatter plots of the RGB map with 1:1 lines. Brighter cells (closer to white) indicate relatively high values for each offset, while darker cells (closer to black) indicate relatively lower values. **(B3)** Comparison of local, reverse, and forward offsets between western and eastern populations. **(C)** Relationship between genomic load and local genomic offset across *P. lasiocarpa* populations: **(C1, C2)** Relationship between two proxies of genetic load (y-axis: the ratio of derived deleterious/loss of function (Lof) variants to derived synonymous variants) and local genetic offset (x-axis). Blue and yellow circles represent western and eastern populations, respectively. The solid blue line denotes the best-fit linear regression line, with light-grey shading representing the 95% confidence interval. **(C3)** Comparison of genomic load between western and eastern populations. Significance

was determined using the two-tailed Wilcoxon test, with significance indicated by asterisks above the boxplot (*** $P<0.001$, ** $P<0.01$, * $P<0.05$, ns: $P>0.05$).

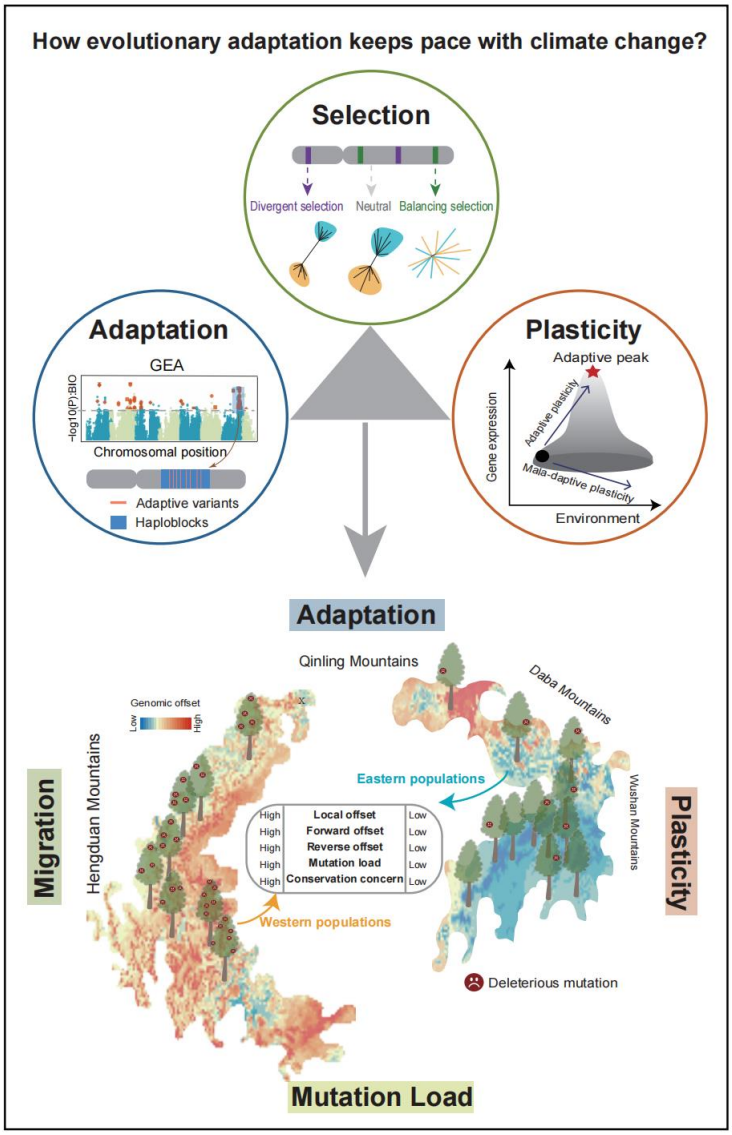

Fig. 7. Schematic illustration of integrating evolutionary genomics to understand the rate of evolutionary adaptation in *P. lasiocarpa* populations in response to climate change. Large-scale population genomics, experimental evolution, and environmental modeling analyses were used in this study to elucidate the roles of evolutionary processes—such as selection, adaptation, and plasticity—in enabling populations to keep pace with climate change. These analyses highlight that western populations, primarily located in the Hengduan Mountains, are the most vulnerable to climate change and thus require priority in conservation and management efforts.